Oxidized low-density lipoprotein potentiates angiotensin II-induced Gq activation through the AT1-LOX1 receptor complex：Implications for renal dysfunction

Jittoku Ihara [1)#], Yibin Huang [1)2)#], Yoichi Takami [1)*], Yoichi Nozato [1)*], Toshimasa Takahashi [1)3)], Akemi Kakino [4)], Cheng Wang [1)], Ziwei Wang [1)], Yu Guo [1)], Weidong Liu [1)], Nanxiang Yin [1)], Ryoichi Ohara [1)], Taku Fujimoto [1)], Shino Yoshida [1)], Kazuhiro Hongyo [1)], Hiroshi Koriyama [1)], Hiroshi Akasaka [1)], Hikari Takeshita [1)], Shinsuke Sakai [5)], Kazunori Inoue [5)], Yoshitaka Isaka [5)], Hiromi Rakugi [1)], Tatsuya Sawamura [4)], and Koichi Yamamoto [1)]

[1] Department of Geriatric and General Medicine, Osaka University Graduate School of Medicine, 2-2 Yamada-oka, Suita, Osaka, 565-0871, Japan

[2] Center for Pulmonary and Vascular Biology, Dept. of Pediatrics, University of Texas Southwestern Medical Center, 5323 Harry Hines Blvd., Dallas, TX, 75390, USA

[3] Department of Medicine, Takahashi clinic, Kobe, Hyogo, 657-0846, Japan

[4] Department of Molecular Pathophysiology, Shinshu University Graduate School of Medicine, Matsumoto, Nagano 390-8621, Japan

[5] Department of Nephrology, Osaka University Graduate School of Medicine, 2-2 Yamada-oka, Suita, Osaka, 565-0871, Japan

#These authors contributed equally to this work.

Correspondence and requests for materials should be addressed to

Yoichi Takami, M.D., Ph.D.*

Department of Geriatric and General Medicine, Osaka University Graduate School of Medicine, #B6, 2-2 Yamadaoka, Suita, Osaka 565-0871, Japan

Tel.: +81-6-6879-3852, Fax: +81-6-6879-3859, E-mail: takami@geriat.med.osaka-u.ac.jp

and

Yoichi Nozato, M.D., Ph.D.*

Department of Geriatric and General Medicine, Osaka University Graduate School of Medicine, #B6, 2-2 Yamadaoka, Suita, Osaka 565-0871, Japan

Tel.: +81-6-6879-3852, Fax: +81-6-6879-3859, E-mail: yoichi.nozato@geriat.med.osaka-u.ac.jp

Keywords: AT1, LOX-1, oxidized LDL, Angiotensin II, Gq, CKD

Abstract

Chronic kidney disease (CKD) and atherosclerotic heart disease, frequently associated with dyslipidemia and hypertension, represent significant health concerns. We investigated the interplay among these conditions, focusing on the role of oxidized low-density lipoprotein (oxLDL) and angiotensin II (Ang II) in renal injury via G protein αq subunit (Gq) signaling. We hypothesized that oxLDL enhances Ang II-induced Gq signaling via the AT1 (Ang II type 1 receptor)-LOX1 (lectin-like oxLDL receptor) complex. Based on CHO and renal cell model experiments, oxLDL alone did not activate Gq signaling. However, when combined with Ang II, it significantly potentiated Gq-mediated inositol phosphate 1 production and calcium influx in cells expressing both LOX-1 and AT1 but not in AT1-expressing cells. This suggests a critical synergistic interaction between oxLDL and Ang II in the AT1-LOX1 complex. Conformational studies using AT1 biosensors have indicated a unique receptor conformational change due to the oxLDL-Ang II combination. In vivo, wild-type mice fed a high-fat diet with Ang II infusion presented exacerbated renal dysfunction, whereas LOX-1 knockout mice did not, underscoring the pathophysiological relevance of the AT1-LOX1 interaction in renal damage. These findings highlight a novel mechanism of renal dysfunction in CKD driven by dyslipidemia and hypertension and suggest the therapeutic potential of AT1-LOX1

55 receptor complex in patients with these comorbidities.

56

57 ## Introduction

58 Dyslipidemia is a major risk factor of atherosclerotic heart disease in patients with chronic
59 kidney disease (CKD). It has been postulated that the association between dyslipidemia
60 and CKD is not solely a result of epidemiological comorbidities but rather a complex
61 interplay of causality, where CKD exacerbates dyslipidemia, while dyslipidemia, in turn,
62 contributes to the onset and progression of CKD[1,2]. Since Moorhead et al. proposed the
63 lipid nephrotoxicity hypothesis in 1982[3], accumulating evidence has suggested that
64 increased plasma lipid levels contribute to the development of renal glomerular and
65 tubular damage, primarily in animal models of dyslipidemia[4]. The etiology of
66 dyslipidemia-induced nephrotoxicity is complex and multifaceted, potentially involving
67 the activation of certain cellular signaling pathways that culminate in renal injury through
68 elevated levels of oxidized LDL (oxLDL)[5-8]. The lectin-like oxLDL receptor, LOX-1, is
69 implicated in organ damage caused by dyslipidemia, and its expression is increased in
70 hypertensive glomerulosclerosis[9]. In murine models, a deficiency of LOX-1 leads to a
71 reduction in renal dysfunction, which was precipitated by a systemic inflammatory state
72 following significant myocardial ischemia and injury[10]. This supports the hypothesis that
73 LOX-1 plays a role in the development of inflammation-induced renal injury. However,
74 to date, no studies have investigated the role of LOX-1 in nephrotoxicity caused by

75 dyslipidemia.

76 Hypertension is an established risk factor for CKD, and it has been suggested that
77 hypertension and dyslipidemia act synergistically to induce renal dysfunction[11]. The
78 development of renal damage due to hypertension involves direct renal injury by
79 vasoactive hormones, such as angiotensin II (Ang II), in addition to renal hemodynamic
80 abnormalities associated with elevated body pressure[12]. We have shown that LOX-1 and
81 the Ang II type 1 receptor (AT1) of the G protein-coupled receptor (GPCR) are coupled
82 on the plasma membrane, and that G protein-dependent and β-arrestin-dependent AT1
83 activation mechanisms are involved in the signaling mechanism by oxLDL and the
84 intracellular uptake of oxLDL, respectively[13,14].

85 Interestingly, it was recently demonstrated that AT1 exhibits different modes and degrees
86 of G protein activation depending on the conformational changes that occur during
87 activation by various ligands[15]. Specifically, G protein αq subunit (Gq)-biased agonists
88 induce a more open conformation of AT1 than Ang II, resulting in a more potent activation
89 of Gq, which is the primary mediator of Ang II-induced hypertension. In contrast, β-
90 arrestin-biased agonists induce a closer conformational change, leading to the activation
91 of β-arrestin without the activation of Gq[15]. Indeed, we found that oxLDL selectively
92 activates G protein αi subunit (Gi) of AT1, without activating Gq[14], similar to that induced

93 by β-arrestin-biased agonists[16]. However, given that Ang II and oxLDL coexist in
94 physiological environments, it is plausible to hypothesize that the effect of these ligands
95 on AT1 in living organisms may differ from their effects when administered individually.
96 Indeed, we found that the combination treatment of oxLDL and Ang II enhanced pro-
97 inflammatory NFκB activity compared to each treatment alone in cells overexpressing
98 both AT1 and LOX-1[14]. Based on our findings and the aforementioned structure-activity
99 relationship of AT1, we hypothesized that the binding of both oxLDL and Ang II to LOX-
100 1 and AT1, respectively, may result in a more open AT1 structure, leading to stronger
101 downstream Gq signaling. Therefore, this study aimed to investigate and clarify this
102 hypothesis, focusing specifically on renal component cells, and ultimately demonstrate
103 the in vivo relevance of this phenomenon in the development of renal injury or renal
104 dysfinction under conditions of Ang II and oxLDL overload.
105
106

Results

Oxidized LDL potentiates Ang II-induced Gq signaling in a LOX-1-dependent manner

First, we examined the additive effect of oxLDL on Ang II-stimulated AT-1-Gq signaling in CHO (Chinese hamster ovary) cells that did not endogenously express LOX-1 and AT-1 but were genetically engineered to express these receptors (CHO-LOX-1-AT1) [13]. Fig. 1a shows the dose-response curve of Ang II-induced IP1 production, which serves as a measure of Gq activity, in the presence of varying concentrations of oxLDL in CHO-LOX-1-AT1 cells. Consistent with previous findings, oxLDL alone did not stimulate IP1 production in CHO-LOX-1-AT1 cells [14]. However, when oxLDL was supplemented at concentrations of 10 and 20 μg/mL (but not at 5 μg/mL), it caused a similar leftward shift in the dose-response curve of Ang II, resulting in a more than 80% decrease in the Effective Concentration 50 (EC50) (EC50 values: 0 μg/mL, 9.40×10^{-9} M; 5 μg/mL, 5.21×10^{-9} M; 10 μg/mL, 1.68×10^{-9} M; 20 μg/mL, 1.55×10^{-9} M). The maximum IP1 production induced by Ang II in CHO-LOX-1-AT1 cells was unaffected by the addition of oxLDL.

Additionally, we observed that oxLDL administration decreased Ang II-induced IP1 production in CHO cells expressing AT1 alone (CHO-AT1), in contrast to CHO cells

125 expressing both AT1 and LOX-1 (Fig. 1b). This finding suggests that the potentiating
126 effect of oxLDL on Ang II-AT1-Gq activity is dependent on the presence of LOX-1.
127 However, the reason for the decrease in IP1 production caused by oxLDL
128 supplementation was not determined in this study. Native LDL, which does not bind to
129 LOX-1, did not alter Ang II-induced Gq activity in CHO-LOX-1-AT1 cells (Fig. 1c).
130 Furthermore, the presence of advanced glycation end products (AGEs) that bind to LOX-
131 1[17], did not enhance Ang II-induced IP1 production (Fig. 1d).
132 We found that enhanced IP1 production by co-treatment of oxLDL with Ang II was
133 similarly observed in CHO-cells expressing LOX-1 and mutated AT1 with impaired
134 ability to activate β arrestin[14] (Fig 1e). Moreover, the potentiating effect of oxLDL on IP1
135 production was unaffected by Pertussis Toxin (PTX), a Gi inhibitor, or RKI-1448, a
136 downstream Rho kinase inhibitor targeting G12/13 signaling in CHO-LOX-1-AT1 cells.
137 However, this phenomenon was completely inhibited by YM-254890, the Gq inhibitor
138 (Fig. 1f). These results suggest that the potentiating effect of oxLDL on Ang II-induced
139 IP1 production is not influenced by β-arrestin, Gi, or G12/13, which are the main effectors
140 of AT1 signaling aside from Gq[18].
141
142 **oxLDL potentiates Ang II-induced calcium influx in a LOX-1-dependent manner**

143 Calcium influx is a representative cellular phenomenon that occurs in response to Ang II-
144 AT1-Gq activation. We found that oxLDL and low concentrations of Ang II (10^{-12} M) did
145 not induce calcium influx in CHO-LOX-1-AT1 cells when treated alone, but apparently
146 induced calcium influx when treated together (Fig. 1g, h). Ang II alone at higher
147 concentrations (10^{-11} M) induced calcium influx, and no further enhancement was
148 observed with oxLDL supplementation (Fig. 1h). The combined effect of oxLDL and Ang
149 II on calcium influx was completely blocked by YM254890, suggesting that this
150 phenomenon was Gq-dependent (Fig. 1i). Importantly, oxLDL supplementation with Ang
151 II did not affect the calcium influx in CHO cells expressing AT1 alone (Fig. 1j).
152

153 **Co-treatment of oxLDL with Ang II induces conformational change of AT1 different**
154 **from each treatment alone**

155 To gain mechanistic insight into this phenomenon, we initially conducted a live-imaging
156 analysis of membrane LOX-1 and AT1 to determine whether the combined treatment of
157 oxLDL and Ang II leads to increased internalization of AT1 upon activation compared to
158 individual treatments, as described in a previous protocol paper[19] (Fig. S1, Supplemental
159 Video, and Fig. 2a).
160 Our findings revealed a decrease in green puncta, which represent AT1-eGFP, upon

161 treatment with Ang II, oxLDL alone, and their co-treatment compared with the control
162 group (Fig. 2a). However, the extent of membrane AT1 reduction was similar across all
163 the treatment groups (Fig. 2a). Consistent with our previous report[14], oxLDL treatment
164 resulted in a reduction in the red puncta representing LOX-1-mScarlet (Fig. 2a).
165 Importantly, co-treatment with oxLDL and Ang II did not further enhance the reduction
166 of red puncta compared to oxLDL treatment alone (Fig. 2a). Based on these findings, it
167 is conceivable that co-treatment with oxLDL and Ang II does not increase the content of
168 activated AT1 compared to individual treatments alone.
169 AT1 intramolecular FlAsH-BRET biosensors were used to detect AT1 conformational
170 changes in CHO cells expressing LOX-1[20]. Among several biosensors previously tested
171 [20], we used two sensors with FlAsH insertion at the third intracellular loop (ICL3P3) and
172 cytoplasmic-terminal tail (C-tailP1) of AT1 that interacts with Renilla luciferase (RlucII)
173 at the end of the cytoplasmic tail (AT1-ICL3P3 and AT1-C-tailP1, respectively), as these
174 sensors were shown to enhance BRET signaling induced by Ang II compared to biased
175 agonists, including SI, SII, DVG, and SBpA[20]. In CHO cells expressing LOX-1 alone
176 (CHO-LOX-1) transduced with lentivirus encoding AT1-C-tailP1, 10^{-5} M Ang II and the
177 combination of Ang II and 10 μg/mL oxLDL induced BRET similarly, whereas oxLDL
178 alone did not alter BRET (Fig. 2b). In contrast, in CHO-LOX-1 cells transduced with

179 AT1-ICL3P3-encoded lentivirus, the combination of Ang II and oxLDL induced BRET
180 more prominently than Ang II alone, whereas oxLDL alone did not alter BRET (Fig. 2c).
181 Furthermore, the difference between oxLDL and the combination treatment was
182 abolished by a neutralizing antibody against LOX-1 (Fig. 2d). These findings suggested
183 that the concomitant binding of oxLDL to LOX-1 and Ang II to AT1 induced a
184 conformational change in AT1 that was distinct from that induced by Ang II or oxLDL
185 alone.
186
187 **Oxidized LDL potentiates Ang II-induced Gq-calcium signaling in renal cells**
188 To confirm the pathophysiological significance of this phenomenon observed in the
189 overexpressing cells, we validated it in cells endogenously expressing LOX-1 and AT1.
190 We found that oxLDL in combination with Ang II did not increase the cellular IP1 content
191 in human umbilical vein endothelial cells (HUVECs), bovine vascular endothelial cells
192 (BACEs), human aortic vascular smooth muscle cells (HAVSMCs), or rat macrophages
193 (A10) (Fig. S2). In contrast, in normal rat kidney epithelial cells (NRK52E) and
194 fibroblasts (NRK49F), the combination of oxLDL and Ang II, but not Ang II alone,
195 increased IP1 accumulation, which was suppressed in the presence of YM-25480, the Gq
196 inhibitor (Fig. 3a, b). IP1 accumulation induced by co-treatment with Ang II and oxLDL

197 was abolished by the siRNA-mediated knockdown of either AT1 or LOX-1 (Fig. 3 c, d;
198 the knockdown efficacy is shown in Fig. S3). Regarding calcium influx, intracellular
199 calcium concentrations were not increased by the treatment of either 10^{-7} M Ang II or low
200 concentration of oxLDL (2 μg/ml) alone (Fig. 3e, left and middle, Fig 3f). In contrast, the
201 combination of Ang II (10^{-7} M) and oxLDL (2 μg/ml) increased intracellular Ca^{2+}
202 concentration (Fig. 3e, right, Fig. 3f). The combined effect on calcium influx was
203 attenuated by the siRNA knockdown of either AT1 or LOX-1 (Fig. 3g). The Gq inhibitor
204 and angiotensin receptor blocker (ARB), Irbesartan, also inhibited this phenomenon (Fig.
205 3h). Calcium influx was not induced by either combination therapy or monotherapy in
206 NRK52E cells (Fig. S4).
207

208 **Co-treatment of oxLDL and Ang II enhanced cellular response upon Gq activation**
209 **in renal cells**

210 In NRK49F cells, co-treatment of oxLDL and Ang II, compared to vehicle, increased
211 mRNA levels of NADPH components, *p67phox* and *p91phox*, fibrosis markers,
212 *fibronectin*, *collagen-1*, *collagen-4*, and *TGFβ*, and inflammatory cytokines, *TNFα*, *IL1β*,
213 *IL-6,* and *MCP-1* (Fig. 4a). Notably, oxLDL did not alter the expression of the genes of
214 interest, and Ang II increased the mRNA levels of only *fibronectin* and *MCP-1*, indicating

215 the apparent synergistic effect of co-treatment with Ang II and oxLDL on specific gene
216 expression. This amplification effect of co-treatment was also observed in limited genes
217 including *p67phox*, *TGFβ, IL-6,* and *MCP-1* in NRK52E cells (Fig. 4b). The combined
218 effects of oxLDL and Ang II on gene expression were completely abolished by the Gq
219 inhibitor (Fig. 4c, d) and ARB (Fig. 4e, f) in NRK49F and NRK 52E. We also verified
220 protein expression of αSMA as a molecular marker of epithelial-mesenchymal transition
221 (EMT) upon the indicated stimulation for 3 days in rat kidney cells. The combination of
222 Ang II (10^{-7} M) and oxLDL (5 μg/mL) induced αSMA expression in NRK49F or NRK52E
223 to the same extent or less than TGFβ, a major inducer of EMT, respectively (Fig. 5a, b).
224 The results of the combination treatment were strikingly different from that of oxLDL or
225 Ang II treatment alone, which did not affect αSMA expression in both types of cells (Fig.
226 5c, d). The induction of αSMA by the combined treatment was suppressed in the presence
227 of a Gq inhibitor or ARB in both types of cells, suggesting the AT1-Gq-dependent
228 pathway in this phenomenon (Fig. 5e, f and Fig. 5g, h). As a final in vitro assay, the
229 proliferative activity of NRK49F cells after 24 h of treatment with Ang II and oxLDL,
230 either alone or in combination, was measured using the BrdU assay (Fig. 6a). When
231 administered alone, Ang II and oxLDL increased and reduced BrdU incorporation,
232 respectively. The reducing effect of oxLDL on proliferation was blocked by Irbesartan,

233 but not by a Gq inhibitor, consistent with our findings that oxLDL induces biased
234 activation of AT1, which favors Gi but not Gq signaling[14]. Oxidized LDL potentiated the
235 Ang II-induced increase in BrdU incorporation, which was blocked in the presence of a
236 Gq inhibitor or an ARB (Fig. 6a). The siRNA-mediated knockdown of AT1 completely
237 abolished the effects of Ang II and oxLDL, either alone or in combination. Knockdown
238 of LOX-1 did not affect the pro-proliferative effect of Ang II itself but blocked the
239 enhanced proliferation induced by co-treatment with oxLDL (Fig. 6b).
240

241 **Oxidized LDL-inducible diet exacerbates Ang II-induced renal dysfuntion in**
242 **wildtype mice, but not in LOX-1 knockout mice.**

243 To examine the relevance of this phenomenon in renal injury, we replicated the in vivo
244 conditions that occurred during simultaneous stimulation with oxLDL and Ang II in
245 wildtype (WT) and LOX-1 knockout (LOX-1 KO) mice. This was achieved by inducing
246 oxLDL via a high-fat diet (HFD) [21] and Ang II via a subcutaneously implanted osmotic
247 mini-pump (Fig. 7a). Two different doses of Ang II were used in the experiment: a pressor
248 dose of 0.7 γ, which was demonstrated to increase blood pressure (BP) and induce renal
249 dysfunction[22,23], and a subpressor dose of 0.1 γ, which does not affect BP. For the intended
250 analysis, the results are presented separately for mice exposed to subpressor and pressor

251 doses of Ang II, utilizing the same outcomes of control animals infused with saline for
252 comparison. Consistent with a previous report, the HFD used in the study prominently
253 increased the plasma LOX-1 ligand concentration, which was undetectable under a
254 normal diet (ND) after 6 weeks of feeding (Fig. S5). Notably, the HFD did not intensify
255 but rather attenuated the body weight increase during the experimental period compared
256 to the ND (Fig. S6a-c). The pressor dose of Ang II similarly increased BP in HFD-fed and
257 ND-fed WT mice (Fig. 7b, Fig. S6d). However, notably, there was a modest trend of
258 attenuated BP elevation by 0.7 γ Ang II infusion in LOX-1 KO mice, in line with the
259 previous report showing reduced Ang II-induced BP elevation by LOX-1 deficiency in
260 mice (Fig. 7b, Fig. S6d, f)[24]. As expected, a subpressor dose of Ang II did not alter BP in
261 the corresponding mouse group (Fig. 7b, Fig. S6e). Regarding biofluid analysis, HFD
262 with saline infusion did not alter the urinary 8-OHdG concentration as a marker of
263 oxidative stress and urinary albumin excretion (UAE) compared to ND with saline
264 infusion in either WT or LOX-1 KO mice (Fig. 7c, d). The pressor dose of Ang II with
265 ND significantly increased the urinary 8-OHdG concentration and UAE in WT mice (Fig.
266 7c, d). Notably, HFD feeding in WT mice with a pressor dose of Ang II resulted in a
267 prominent increase in urinary 8-OHdG concentration and UAE compared to mice fed
268 with ND (Fig. 7c, d). In WT mice administered with a subpressor dose of Ang II, a

269 significant increase in UAE was observed when comparing the effects of HFD to ND (Fig.
270 7d). There were no significant differences in urinary 8-OHdG levels between the two
271 dietary conditions (Fig. 7c). Interestingly, when LOX-1 KO mice were fed either HFD or
272 ND and then administered the corresponding dose of Ang II, no differences were observed
273 in the measured parameters (Fig. 7c, d). These findings indicate that the combination of
274 HFD and Ang II administration appears to have a more pronounced effect on certain
275 biofluid markers of renal injury in WT mice than in LOX-1 KO mice. The presence or
276 absence of LOX-1 appears to influence the interaction between HFD and Ang II, affecting
277 these specific parameters in mice. We did not find a difference in plasma aldosterone
278 concentration between ND- and HFD-fed WT mice with a pressor dose of Ang II (Fig.
279 S7).
280 We then conducted quantitative real-time PCR analysis on genes within kidney sections,
281 encompassing NADPH components (*p40phox, p47phox, p67phox, and p91phox*),
282 inflammatory cytokines (*IL-6, TNFα, IL1β, MCP-1, and COX-2*), fibrosis markers (*TGFβ,*
283 *fibronectin, collagen-1a, collagen-4a, αSMA, and vimentin*), epithelial markers (*E-*
284 *cadherin and cadherin-16*), and tubular marker (*NAGL*) (Fig. 8, Fig S8). In mice treated
285 with a pressor dose of Ang II, 15 out of 18 genes examined showed enhanced alterations
286 in gene expression, indicative of heightened NADPH oxidase components, inflammatory

287 cytokines, fibrosis, decreased epithelial markers, and exacerbated tubular injury in HFD-
288 fed WT mice compared to ND-fed mice (Fig. 8a, Fig. S8a). For many of these genes, a
289 synergistic effect of the combination of a pressor dose of Ang II and HFD was not
290 observed in LOX-1 KO mice (Fig. 8a, Fig. S8a). Seven genes displayed discernible
291 differences between HFD- and ND-fed WT mice treated with a subpressor dose of Ang
292 II (Fig. 8b Fig. S8b). Other than *fibronectin*, no differences were observed between ND-
293 and HFD-fed LOX-1 mice exposed to a subpressor dose of Ang II (Fig. 8b Fig. S8b). In
294 relation to AT1 and LOX-1 expression, no variations emerged between the ND and HFD
295 groups when subjected to the corresponding dose of Ang II treatment in both WT and
296 LOX-1 KO mice (Fig. S8a, b).
297 In the histological analysis of kidney samples, in contrast to the gene expression data, the
298 administration of either a subpressor or pressor dose of Ang II, both in isolation and in
299 combination with HFD for 4 weeks, did not reveal any notable increase in fibrosis, as
300 evaluated by Masson-Trichrome staining (Fig. S9a). Similarly, there was no significant
301 change in the degree of mesangial expansion or glomerular area, as assessed by PAS
302 staining. (Fig. S9b).
303 Finally, immunofluorescence staining of mouse kidney specimens was performed to
304 detect the colocalization sites of LOX-1 and AT1 in the kidney. As shown in Fig. 9a and

305 Fig. 9b, LOX-1 and AT1a were predominantly colocalized in the renal tubules, but not in

306 the glomeruli.

307

308

309

310

311

312

313

314

315

316

317

318

319

320

321

322

323 **Discussion**

324 We conducted a series of experiments to provide empirical support for our hypotheses.
325 We propose that the simultaneous binding of Ang II to AT1 and oxLDL to LOX-1 triggers
326 distinct and more pronounced structural modifications in AT1 than the individual
327 modifications induced by each ligand. This structural alteration in AT1 leads to the
328 enhanced activation of Gq signaling.

329 Our experiments showed that oxLDL enhanced the effects of Ang II-induced production
330 of IP1, a downstream signaling molecule associated with Gq activation and subsequent
331 calcium influx. However, this effect was observed only in the presence of both LOX-1
332 and AT1. Considering that oxLDL selectively activates Gi but not Gq through the LOX-
333 1-AT1 dependent pathway[14], it is evident that the observed phenomenon cannot be
334 attributed solely to the additive effect of oxLDL on AT1 activation. Rather, the
335 simultaneous binding of oxLDL and Ang II to their respective receptors, LOX-1 and AT1,
336 which form a single complex, underlies this phenomenon. Indeed, our findings from live
337 imaging of the membrane receptors revealed that the combination of Ang II and oxLDL
338 did not induce any additional influence on the internalization of both receptors upon AT1-
339 β-arrestin activation compared to each ligand alone, suggesting that the quantity of
340 activated receptors is not affected by the combination treatments. Considering the

341 conformation-activation relationship in AT1 activation[20], this supports the hypothesis that
342 the simultaneous binding of Ang II and oxLDL in a single AT1-LOX-1 complex induces
343 a greater conformational change, resulting in a more open conformation of AT1 compared
344 with each ligand alone. However, it is technically challenging to directly identify
345 structural modifications of the receptor complex using techniques such as crystal structure
346 analysis. Instead, we utilized AT1 conformational sensors capable of differentiating
347 between the conformational changes induced by Ang II and biased AT1[20]. Interestingly,
348 we observed that one of the two conformational sensors employed in this study detected
349 an augmented response in the presence of the combination treatment compared with Ang
350 II alone. Importantly, this enhanced response was significantly inhibited when an LOX-1
351 antibody was introduced, indicating the dependency of LOX-1 on this phenomenon.
352 These results indicate that the combined treatment with Ang II and oxLDL in the presence
353 of LOX-1 induces a unique conformational change in individual AT1 molecules, which
354 differs from the conformational changes induced by each single treatment alone.
355 It is important to note that the ability of LOX-1 ligands to enhance Ang II-AT1 signaling
356 is not commonly observed. This was corroborated by the observation that BSA-
357 conjugated AGE, a recognized ligand of LOX-1[17], failed to augment the production of
358 IP1 by Ang II compared to control BSA (Fig. 1d). While the exact reason for this

359 discrepancy is not yet understood, it is noteworthy that the predicted particle size of
360 oxLDL[25] is significantly larger at 250 Å compared to the maximum particle size of AGE-
361 BSA[26], which is 120 Å. This suggests a potentially greater impact of oxLDL on the
362 structural modifications within the AT1-LOX-1 complex. However, further structural
363 analysis is required to validate this hypothesis.

364 Notably, the Gq bias resulting from combination treatment varied across the mammalian
365 cells examined. Specifically, we observed a combinatorial effect exclusively in renal
366 epithelial and fibroblasts, whereas vascular endothelial and smooth muscle cells did not
367 display the same response. In these renal cells, we observed increased Gq signaling, along
368 with other cellular phenomena such as calcium influx, changes in gene expression, and
369 alterations in cellular characteristics, including EMT and cell proliferation. Specifically,
370 EMT is an important cellular phenomenon in renal epithelial cells to acquire the
371 phenotype of myofibroblasts and induce fibrosis by the excessive production and
372 deposition of extracellular matrix (ECM) proteins, although there is a debate regarding
373 the precise role of EMT in vivo[27]. Numerous studies have suggested that the EMT plays
374 a critical role in Ang II-mediated renal fibrosis. EMT is also involved in the pathological
375 transition of normal fibroblasts to myofibroblasts, which promotes fibrosis. We found that
376 αSMA expression, a well-known indicator of EMT, was dramatically enhanced when

377 renal epithelial cells and fibroblast cells were subjected to the combination treatment of
378 Ang II and oxLDL, in comparison to individual treatments. Additionally, fibroblast
379 proliferation, as assessed by the BrdU assay, was notably enhanced by the combined
380 treatment, as opposed to each treatment administered separately. Interestingly, the use of
381 5 μg/mL oxLDL in our study showed a tendency to decrease proliferation, which was
382 counteracted by the administration of an ARB but not a Gq inhibitor. These findings
383 suggest that the presence of Ang II leads to a significant transformation in the function of
384 oxLDL, primarily due to its altered influence within the AT1-LOX-1 complex. Taken
385 together, these results suggest that the simultaneous binding of oxLDL to LOX-1 and Ang
386 II to AT1 results in a Gq-biased shift in AT1 activation, leading to a cellular phenomenon
387 that could potentially contribute to renal damage.
388 In an animal study, we introduced a biological environment in which both circulating Ang
389 II and oxLDL (an LOX-1 ligand) were increased in mice. Previous studies using mice fed
390 an HFD have consistently reported the onset of renal injury, as determined by various
391 measurements[28-32]. In contrast, 6 weeks of HFD feeding without Ang II treatment did not
392 alter renal function in our mice. This can be attributed to the lack of obesity induced by
393 the high-fat diet in this study. We used this diet based on a previous study that confirmed
394 increased circulating LOX-1 ligand levels without body weight gain in mice[33], and this

395 diet decreased body weight in our experiments. Obesity is a well-established and
396 clinically proven risk factor of renal dysfunction. The mechanisms underlying this
397 association are complex and involve various factors other than lipid abnormalities, such
398 as hemodynamic changes that affect kidney circulation and the impact of adipose tissue
399 on the production of adipokines and other inflammatory mediators[34,35]. Consequently, we
400 observed the influence of elevated lipid particle levels on renal function, independent of
401 obesity. We found that the effect of an HFD became obvious with an increase in the Ang
402 II load in WT mice. In particular, in WT mice treated with high-dose Ang II, which
403 elevated systolic BP by approximately 30 mm Hg, an HFD induced notable increases in
404 urinary reactive oxygen species and urinary albumin. In contrast, an HFD had no impact
405 on Ang II-infused LOX-1 KO mice, as evidenced by equivalent urinalysis measurements
406 for renal injury between the diets. Correspondingly, simultaneous administration of an
407 HFD and Ang II resulted in a consistent alteration in the expression of genes related to
408 renal injury, including fibrosis, inflammation, and oxidative stress, except for some genes
409 in WT mice, but not in LOX-1 KO mice. This strongly suggests that the combined effect
410 of Ang II and HFD on renal function is LOX-1 dependent. Nevertheless, it should be
411 noted that the effect of high-dose Ang II infusion on BP tended to be less pronounced in
412 LOX-1 KO mice compared to WT mice, although there were no differences in BP

413 elevation between the diets in each group of mice. These findings align with those of
414 previous studies indicating that LOX-1 knockout mice show resistance to Ang II-induced
415 elevation of BP[24,36,37]. Specifically, when mice were infused with 2 γ Ang II (equivalent
416 to 25 g mice) for a duration of 28 days, wildtype mice experienced a BP increase
417 exceeding 180 mmHg, while LOX-1 knockout mice demonstrated a reduction of
418 approximately 40 mmHg in this elevation[24]. Furthermore, the same research group
419 reported that Ang II infusion led to less severe renal injury in LOX-1KO mice compared
420 to WT mice[36]. Importantly, these findings were observed in mice fed with an ND,
421 suggesting that the protective effect of LOX-1 loss-of-function against Ang II-induced
422 elevated BP occurs through the LOX-1-AT1 complex, independent of the presence of
423 oxLDL. Taken together, the effects of LOX-1 on AT1 signaling are complex, involving
424 both ligand-dependent and -independent mechanisms, and further investigation is
425 required for a comprehensive understanding of the LOX-1-AT1 interaction.
426 Finally, the current findings unequivocally demonstrated the molecular interactions
427 between key molecules associated with dyslipidemia and hypertension in the kidneys.
428 Moreover, this interaction can be effectively inhibited by ARBs, suggesting an additive
429 effect in preventing the development of CKD, particularly in patients with hypertension
430 and dyslipidemia. Interestingly, Ang II-dependent hypertensive animal models, including

431 constriction of the renal artery and infusion of Ang II in rats and mice, have revealed a
432 progressive increase in intrarenal Ang II levels, surpassing what can be accounted for by
433 circulating Ang II levels alone[38]. This is due to Ang II-dependent renal activation of the
434 renin-angiotensin system, as indicated by increased urinary angiotensinogen (AGT)
435 secretion[38,39]. Importantly, the elevation of urinary AGT is also evident in patients with
436 various pathologies, including hypertension and CKD, implying that renal Ang II levels
437 increase even in individuals who do not exhibit elevated levels of circulating Ang II[21,39,40].
438 Taken together, the current finding of the synergistic effect of Ang II and oxLDL on AT1
439 activation in renal tissue is highly relevant for the development of kidney disease. RA
440 system inhibitors, ARB, and ACE inhibitors are prioritized therapies to prevent the
441 development of CKD with proteinuria in patients with hypertension[41]. In addition to the
442 well-established inhibitory effects of Ang II on the contraction of efferent arterioles[42], a
443 novel renal protective action of RA system inhibitors has been proposed. Particularly in
444 hypertension accompanied by dyslipidemia, RA system inhibitors may exhibit anti-
445 inflammatory, antifibrotic, and antioxidant effects in the kidneys by inhibiting the Gq
446 signaling pathway through the AT1-LOX-1 complex in renal tubular cells and fibroblasts.
447 Collectively, the current findings suggest that RA inhibitors can concomitantly reduce the
448 effect of increased renal Ang II and oxLDL levels on the development of CKD in patients

449 with hypertension and dyslipidemia, although direct evidence in clinical studies to
450 support this remains to be elucidated.
451 This study has several limitations as follows: 1) The kidney, a complex organ vital for
452 maintaining homeostasis, comprises a myriad of distinct cell types working in concert to
453 execute its multifaceted functions[43]. The experiments conducted in mice raised questions
454 regarding the specific cell types implicated in the synergistic effect of Ang II and oxLDL
455 within the LOX-1-AT1 complex in the kidney. Addressing this issue would ideally require
456 single-cell analysis, which is a challenge for future research. 2) The study employed
457 systemic LOX-1 knockout mice. For a more detailed analysis, a phenotypic investigation
458 using renal tissue-specific LOX-1 and AT1 knockout mice is required. Of particular
459 importance is the analysis using tubule-specific knockout mice, in which the localization
460 of these components has been verified through immunohistochemical staining. 3) The
461 administration of Ang II (both pressor and subpressor doses) and its combination with
462 HFD did not result in any histological changes in terms of fibrosis and mesangial
463 expansion, despite the observed alterations in the associated gene expression and
464 urinalysis for renal injury. Alterations in gene expression and urinalysis for renal injury
465 may be sensitive and relatively early phenomena, and this discrepancy could potentially
466 be attributed to the relatively short intervention duration of 4 weeks. Therefore,

467 concurrent pathohistological alterations in the renal tissue might become evident with a
468 more extended intervention period. 4) This study was limited by its inability to detect the
469 amplification of Gq signaling in mouse renal tissue due to the concurrent administration
470 of Ang II and HFD. Overcoming this limitation is a challenge for future studies.
471 In conclusion, the current findings suggest that the simultaneous binding of oxLDL and
472 Ang II to their respective receptors within the complex induces a distinct conformational
473 change compared with the effect of each ligand alone. This unique conformational change
474 results in the heightened activation of G protein signaling and subsequent unfavorable
475 cellular reactions in renal component cells. The relevance of this phenomenon was
476 confirmed in mouse models, in which renal dysfunction was prominently exacerbated
477 when there was a concomitant increase in Ang II and oxLDL levels. Notably, this effect
478 was abolished by the deletion of LOX-1, indicating LOX-1 dependency of this in vivo
479 phenomenon (Fig. 10). These findings indicate the clinical relevance of the direct
480 interaction between hypertension and dyslipidemia and further support the clinical
481 significance of RA inhibition in treating patients with CKD.
482
483
484

485 ## Materials and methods

486 **Cell culture and materials**

487 HUVECs and BAECs were cultured in EGM-2 (Lonza, Basel, Switherlad). Cells with
488 fewer than five passages were used in the experiments. Transgenic CHO cells were
489 maintained in an F-12 Nutrient Mixture with GlutamaxTM-I (Thermo Fisher Scientific,
490 MA, USA), 10% fetal bovine serum (FBS; Gibco, USA), and appropriate selection
491 reagents, as described below. CHO-K1 cells were maintained in F-12 Nutrient Mixture
492 with GlutamaxTM-I and 10% FBS. HAVSMCs were cultured in Dulbecco's modified
493 Eagle's medium/F12 (DMEM/F12) (Nacalai Tesque, Japan) supplemented with 1%
494 penicillin-streptomycin (Fujifilm, Japan) and 10% FBS. A10 cells were grown in DMEM
495 (Wako, Osaka, Japan) supplemented with 10% FBS and 1% penicillin-streptomycin.
496 NRK52E and NRK49F cells (ECACC, UK) were cultured in DMEM (Wako, Japan)
497 supplemented with 5% FBS and the appropriate selection reagents. Gene transcription in
498 CHO cells was induced by adding 100 ng/mL doxycycline (Merck KGaA, Darmstadt,
499 Germany). Cells were incubated at 37℃ in 5% CO_2 and 95% air.

500

501 **Construction of plasmid vectors**

502 For stable transformants, pTRE2hyg vector (Clontech, USA) encoding mutated hAT1

503 with impaired ability to activate β-arrestin (pTRE2hyg-HA-FLAG-hAT1mg) were
504 created using site direct mutagenesis as previously described[14]. For real-time imaging,
505 LOX-1 tagged with V5-6×His at the C-terminus (V5-LOX-1) was subcloned into
506 pmScarlet_C1 (plasmid #85042; Addgene) (mScarlet-LOX-1). HA-FLAG-hAT1 was
507 subcloned into pcDNA3-EGFP (plasmid #85042; Addgene) (AT1-eGFP)[14].
508
509 **Stable transformants**
510 We constructed CHO-K1 cells expressing tetracycline-inducible human LOX-1 tagged
511 with V5-6×His at the C-terminus (CHO-LOX-1), human HA-FLAG-hAT1 (CHO-AT1),
512 or cells expressing both human LOX-1 and AT1 (CHO-LOX-1-AT1), as previously
513 described[13,14] To establish cells expressing both LOX-1 and mutated AT1 (pTRE2hyg-
514 HA-FLAG-hAT1mg), they were co-transfected with the pSV2bsr vector (Funakoshi,
515 Japan) into CHO-LOX-1 using the Lipofectamine 2000 transfection reagent (Thermo
516 Fisher Scientific, USA). The stable transformants were selected with 400 μg/mL of
517 hygromycin B (Wako, Osaka, Japan) and 10 μg/mL of blasticidin S (Funakoshi, Japan).
518 The resistant clone expressing LOX-1 and mutated AT1 in response to doxycycline
519 (Calbiochem, USA) was selected for use in the experiments (CHO-LOX-1-AT1mg) [14].
520

521 **Small interfering RNA**

522 NRK52 and NRK47 cells were plated at 50% confluence on the day of transfection.
523 Silencer Select small interfering RNA (siRNAs) for *LOX-1* and *AT1a* (Thermo Fisher
524 Scientific, MA, USA) were transfected into cells in medium without serum or antibiotics
525 using Lipofectamine RNAiMAX (Thermo Fisher Scientific, MA, USA), according to the
526 manufacturer's instructions.

527

528 **Preparation of oxLDL**

529 Human plasma LDL (1.019-1.063 g/mL), isolated by sequential ultracentrifugation,
530 was oxidized using 20 μM $CuSO_4$ in PBS at 37 °C for 24 h. Oxidation was terminated
531 by adding excess EDTA. LDL oxidation was analyzed by agarose gel
532 electrophoresis for migration versus LDL[13].

533

534 **Quantification of cellular IP1 accumulation**

535 Gq-dependent activation of phospholipase C was quantified by measuring IP1 using the
536 IP-One assay kit (Cisbio, France) as previously described[19]. Briefly, cells were seeded at
537 80,000 cells/well in 96 well transparent cell culture plates and incubated under serum-
538 free conditions for 24 h. Thereafter, cells were treated for 1 h with IP1 stimulation buffer,

539 including vehicle, native LDL, oxLDL, Ang II, AGE, PTX
540 (Merck KGaA, Darmstadt, Germany), YM-254890 (Fujifilm Wako, Osaka, Japan), and
541 RKI-1448 (Selleck, USA), as described in the text. Cell lysates with Triton X at a final
542 concentration of 1% were transferred to a 384-well white plate, and IP1 levels were
543 measured by incubating the cell lysates with FRET reagents (cryptate-labeled anti-IP1
544 antibody and d2-labeled IP1 analog).
545
546 **Quantitative real-time PCR**
547 RNA samples were purified using RNeasy Mini Kit (Qiagen, Germantown, MD, USA).
548 One microgram of RNA was converted into cDNA using a ReverTra Ace qPCR RT kit
549 (TOYOBO, Osaka, Japan) according to the manufacturer's instructions. All genes were
550 evaluated using the ViiA7 Real-Time PCR System (Applied Biosystems, Thermo Fisher
551 Scientific, Waltham, MA, USA). The data were analyzed using the ΔΔCt method with
552 normalization against the GAPDH RNA expression in each sample. The primer sequences
553 are listed in the Supplemental Table.
554
555 **Western blotting**
556 Proteins were separated using sodium dodecyl sulfate-polyacrylamide gel electrophoresis

557 and electrophoretically transferred onto polyvinylidene fluoride membranes. The
558 membranes were blocked with 5% nonfat dried milk and incubated with primary
559 antibodies overnight at 4 ºC. The primary antibodies used in this study were as follows:
560 anti-SMA antibody (1:1000), anti-α-Tubulin antibody (1:1000) (Cell Signaling
561 Technology, Inc, Danvers, MA, USA). The bands were visualized with a
562 chemiluminescence detection system (LAS-4000 mini; GE Healthcare Life Sciences,
563 Buckinghamshire, UK) using Chemi-Lumi One Super (Nacalai Tesque, Kyoto, Japan).
564

565 **Calcium influx assay**

566 Calcium influx was measured using Fura 2-AM (Dojindo, Kumamoto, Japan) with slight
567 modifications to the manufacturer's protocol. In brief, cells plated in 96 wells were
568 incubated with 5 μM Fura 2-AM in HEPES buffer saline (20 mM HEPES, 115 mM NaCl,
569 5.4 mM KCl, 0.8 mM MgCl2, 1.8 mM $CaCl_2$, 13.8 mM glucose, pH 7.4) for 1 h at 37°C,
570 followed by replacement with recording medium without Fura 2-AM. Cells were treated
571 with oxLDL, Ang II, or a combination of both at the indicated concentrations. Changes
572 in F340/F380, an index of intracellular calcium concentration, were measured by dual-
573 excitation microfluorometry using a digital image analyzer (Aquacosmos; Hamamatsu
574 Photonics, Hamamatsu, Japan).

575

576 **BrdU assay**

577 Proliferative activity was assessed using a BrdU Cell Proliferation ELISA Kit (Funakoshi,
578 Japan). NRK49F cells were seeded in 96-well tissue culture plates and incubated with the
579 test reagents for 24 h. After incubating the cells with BrdU, we fixed the cells and
580 denatured their DNA using a Fixing Solution. The plate was washed thrice with Wash
581 Buffer before adding the Detector Antibody. Next, 100 μL/well of anti-BrdU monoclonal
582 Detector Antibody was added, and the plate was incubated for 1 h at room temperature.
583 Subsequently, 100 μL/well of Goat Anti-Mouse IgG Conjugate was pipetted and
584 incubated for 30 minutes at room temperature. After five washes, the reaction was stopped
585 by adding Stop Solution to each well. The color of the positive wells changed from blue
586 to bright yellow. Finally, the plate was read at a wavelength of 450/550 nm using a
587 spectrophotometric microtiter plate reader.

588

589 **Creation of lentivirus encoding AT1 conformational sensors**

590 For lentivirus encoding AT1 conformational sensors, rat AT1 and RlucII were subcloned
591 into the pLVSIN-CMV Neo vector (Takara Bio, Japan). Next, the FlAsH binding
592 sequence (CCPGCC) was inserted between residues K135 and S136 in the third

593 intracellular loop (AT1-ICL3P3), as well as between residues K333 and M334 in the
594 cytoplasmic-terminal tail (AT1-Ctail), utilizing the KOD-Plus Mutagenesis Kit (Toyobo,
595 Japan), at the same site as previously documented[14].
596
597 **Intramolecular FlAsH Bioluminescence resonance energy transfer assay to detect**
598 **AT1 conformational change**
599 CHO-LOX-1 cells were initially plated onto a white clear-bottom 96-well culture plate at
600 a density of $1x10^5$ cells/well. The following day, the cells were transduced with lenti-
601 virus encoding AT1-Ctail or AT1-ICL3P3 [20] in 10% FBS. After 24 h of transduction, the
602 cultures were transferred to serum-free conditions and incubated for an additional 24 h.
603 Add 1.5 μM FlAsH-EDT_2 labeling reagent of TC-FlAsH™ II In-Cell Tetracysteine Tag
604 Detection Kit (Thermo Fisher Scientific, MA, USA), wash twice with 250 μM BAL buffer,
605 and assays were promptly conducted on a Spark® microplate reader (TECAN,
606 Switzerland). The BRET ratio (emission mVenus/emission Rluc) was calculated as
607 follows: Following a 3-minute baseline reading (with the final baseline reading presented
608 at 0), cells were exposed to vehicle, oxLDL alone, AII alone, a combination of AII and
609 oxLDL, or a combination of AngII, oxLDL, and LOX-1 antibodies. The BRET ratios
610 were calculated every 16 seconds for a total of 320 seconds and the relative change in

611 intramolecular BRET ratio was calculated by subtracting the average BRET ratio
612 measured for cells stimulated with vehicle at each time point.
613
614 **Analysis of LOX-1 and AT1 dynamics by real-time imaging**
615 Live imaging was performed using previously reported methods[19]. Briefly, twenty-four
616 hours prior to imaging experiments, CHO-K1 cells were transfected with LOX-1-
617 mScarlet and AT1-eGFP by electroporation. Subsequently, the cells were seeded in a 35-
618 mm glass base dish (Iwaki, Japan) that had been pre-coated with a 1000X diluted solution
619 of 10 mg/mL poly-L-lysine (ScienCell, USA) one hour before seeding. The growth
620 medium was substituted with imaging buffer (pH 7.4), which consisted of 125 mM NaCl,
621 5 mM KCl, 1.2 mM $MgCl_2$, 1.3 mM $CaCl_2$, 25 mM HEPES, and 3 mM D-glucose, with
622 the pH adjusted to 7.4 using NaOH. Dynamic images of the cells were acquired at 25 °C
623 using a SpinSR10 inverted spinning disk-type confocal super-resolution microscope
624 (Olympus, Japan). The microscope was equipped with a 100x NA1.49 objective lens
625 (UAPON100XOTIRF, Olympus, Japan) and an ORCA-Flash 4.0 V2 scientific CMOS
626 camera (Hamamatsu Photonics KK, Japan) at 5-second intervals. The imaging
627 experiment was conducted using CellSens Dimension 1.11 software, employing a 3D
628 deconvolution algorithm (Olympus, Japan), and the number of puncta was determined

629 using ImageJ1.53K[19].

630

631 **Animals and diets**

632 Male WT mice (C57BL/6J) and LOX-1 KO mice with a C57BL/6 background were used
633 in this study. LOX-1 KO mice were generated as described previously[44]. Mice were
634 housed in a temperature-controlled (20-22°C) room on a 12 hours light/dark cycle and
635 fed an ND (MF; Oriental Yeast, Osaka, Japan) or an HFD (High Fat Diet without DL-α-
636 tocopherol, CLEA Japan Inc, Tokyo, Japan), which reported to increase plasma LOX-1
637 ligand in ApoE KO mice[21]. All study protocols were approved by the Animal Care and
638 Use Committee of Osaka University and were conducted according to the guidelines of
639 the NIH for the Care and Use of Laboratory Animals.

640

641 **Blood pressure measurement in mice**

642 The blood pressure of the mice was measured using the tail- cuff method with BP-98A
643 (Softron, Japan). The measurements were performed after restraining the mice. The blood
644 pressure was calculated as the average of 6 readings for each animal at each time point.

645

646 **Urine tests in mice**

647 Urine tests in mice included the measurement of urine 8-OHdG, creatinine, and albumin
648 concentrations. The DNA Damage (8-OHdG) ELISA Kit (StressMarq Bioscience,
649 Canada), Creatinine Kit L type Wako (Fujifilm, Japan), and Mouse Albumin ELISA Kit
650 (Bethyl Laboratories, Inc., TX, USA) were utilized for these measurements, following
651 their respective instructions.
652
653 **Plasma LOX-1 ligand concentration**
654 Measurement of LOX-1 ligands containing apoB (LAB) in mouse plasma was performed
655 using a modified protocol based on a previously reported method [33]. Briefly, recombinant
656 human LOX-1 (0.25 μg/well) was immobilized on 384 well plate (greiner, Frickenhausen,
657 Germany) by incubating overnight at 4°C in 50 μl of PBS. After three washes with PBS,
658 80 μl of 20% (v/v) ImmunoBlock (KAC, Kyoto, Japan) was added, and the plates were
659 incubated for 2 h at 25°C. After three washes with PBS, the plates were incubated for 2 h
660 at 25°C with 40 μl of standard oxidized LDL or samples. Samples were prepared by 4-
661 fold dilution of plasma with HEPES-EDTA buffer (10 mM HEPES, 150 mM NaCl, 2 mM
662 EDTA, pH 7.4), and standards were prepared by dilution of oxidized LDL with HEPES-
663 EDTA buffer. Following three washes with PBS, the plates were incubated for 1 h at 25°C
664 with chicken monoclonal anti-apoB antibody (HUC20, 0.5 μg/mL) in HEPES-EDTA

665 containing 1% (w/v) BSA. After three washes with PBS, the plates were incubated for 1
666 h at 25°C with peroxidase-conjugated donkey anti-chicken IgY (Merck, NJ, USA) diluted
667 5000 times with HEPES-EDTA containing 1% (w/v) BSA. After five washes with PBS,
668 the substrate solution containing 3,3',5,5'-tetramethylbenzidine (TMB solution, Bio-Rad
669 Laboratories, CA, USA) was added to the plates and incubated them for 30 min at room
670 temperature. The reaction was terminated with 2 M sulfuric acid. Peroxidase activity was
671 determined by measuring absorbance at 450 nm using a SpectraMax 340PC384
672 Microplate Reader (Molecular Devices, CA, USA).
673
674 **Tissue preperation**
675 Kidneys were perfused with cold PBS before removal. Kidney samples were rapidly
676 excised. A quarter of samples were stored at 4°C in RNAlater (Thermo Fisher Scientific,
677 MA, USA) for RNA extraction. The remaining quarters were fixed in 4%
678 paraformaldehyde overnight at 4°C for histological evaluation. The remaining half was
679 snap-frozen in liquid nitrogen and stored at -80°C for further analysis.
680
681 **Periodic acid-Schiff and Masson-Trichrome staining**
682 The degree of glomerular mesangial expansion and glomerular area (representing the

683 structural integrity of the glomeruli) were assessed in a blinded manner using periodic
684 acid-Schiff (PAS) staining. Collagen accumulation was determined by Masson-Trichrome
685 (MTC) staining. For MTC staining, the area displaying fibrosis was quantitatively
686 evaluated in a blinded manner by measuring the blue staining in six strongly magnified
687 fields of view using the ImageJ software, and the average was calculated after
688 determining the ratio of the total area.
689
690 **Fluorescent immunostaining**
691 For fluorescent immunostaining of LOX-1 and AT-1, the mice were perfused with cold
692 saline before tissue removal. After 3 days of zinc fixation, the tissue was replaced with
693 70% ethanol. The 3-μm-thick kidney tissue sections were immunohistochemically stained
694 with antibodies against ATGR (1:200, Cosmo Bio, Japan) and OLR-1 (1:200, TS58 from
695 the laboratory of T.S., Shinshu University School of Medicine, Nagano, Japan).
696 Following deparaffinization (using Lemosol and gradient ethanol) and rehydration, the
697 slices were subjected to antigen retrieval by autoclaving in citrate buffer (0.01 M; pH 6.0).
698 Subsequently, the slices were washed thrice with PBS and blocked with 5% bovine serum
699 albumin for 30 min at room temperature. The slides were then incubated with primary
700 antibodies for 2 h at room temperature. Goat anti-Rabbit IgG (H+L) High Cross-

Adsorbed Secondary Antibody, Alexa Fluor Plus 488 and 594 (Thermo Fisher Scientific, MA, USA) were used as secondary antibodies for ATGR and OLR-1, respectively. After incubation with secondary antibodies for 1 h at room temperature, the slices were washed with PBS. Finally, slides were sealed and photographed. Visual analyses were performed using a BZ-800L microscope (Keyence, Japan).

Statistical analyses

All data are presented as the mean ± SEM. Differences between two treatments or among multiple treatments were determined using the Student's t-test or one-way ANOVA followed by Tukey's multiple comparison test.

Data availability

All data supporting the findings of this study are available within the paper and its Supplementary Information. Source data are provided in this paper.

Acknowledgements

This work was partially supported by JSPS KAKENHI Grant Numbers 21K07389 (Y.T.), 22K08181 (Y.N.), 20H03576 (H.R.), and 18H02732 (K.Y.). We are grateful to Tomoko

Sato, Yoshinori Koishi, and Chika Takana for technical assistance. We would like to thank Editage (www.editage.com) for the English language editing.

Author contributions

J.I., Y.H., Y.T., Y.N., T.T., and K.Y. designed the study. J.I. and Y.H. performed most of the experiments. A.K. measured plasma LOX-1 ligand concentrations in mice and assisted with data analysis. J.I. and S.S. performed histological analysis of the renal tissue of mice. J.I., Y.H., Y.T., Y.N., T.T., and K.Y. wrote the manuscript and analyzed the data. C.W., Z.W., G.Y., L.W., Y.N., R.O., T.F., H.K., K.A., H.T., S.S., and K.I. analyzed the data and contributed to the discussion. A.K., Y.I., H.R., and T.S. contributed to the discussion and reviewed and edited the manuscript. All authors contributed to the editing of the final manuscript. Y.T. and Y.N. had full access to all data in the study and took responsibility for the integrity of the data and accuracy of the data analysis.

Competing interests

The authors declare no competing interests.

737 **References**

738 1 Harper, C. R. & Jacobson, T. A. Managing dyslipidemia in chronic kidney disease.
739 *J Am Coll Cardiol* **51**, 2375-2384 (2008).
740 https://doi.org/10.1016/j.jacc.2008.03.025

741 2 Cases, A. & Coll, E. Dyslipidemia and the progression of renal disease in chronic
742 renal failure patients. *Kidney Int Suppl*, S87-93 (2005).
743 https://doi.org/10.1111/j.1523-1755.2005.09916.x

744 3 Moorhead, J. F., Chan, M. K., El-Nahas, M. & Varghese, Z. Lipid nephrotoxicity
745 in chronic progressive glomerular and tubulo-interstitial disease. *Lancet* **2**, 1309-
746 1311 (1982). https://doi.org/10.1016/s0140-6736(82)91513-6

747 4 Ruan, X. Z., Varghese, Z. & Moorhead, J. F. An update on the lipid nephrotoxicity
748 hypothesis. *Nat Rev Nephrol* **5**, 713-721 (2009).
749 https://doi.org/10.1038/nrneph.2009.184

750 5 Bussolati, B. *et al.* Statins prevent oxidized LDL-induced injury of glomerular
751 podocytes by activating the phosphatidylinositol 3-kinase/AKT-signaling
752 pathway. *J Am Soc Nephrol* **16**, 1936-1947 (2005).
753 https://doi.org/10.1681/ASN.2004080629

754 6 Dai, Y. *et al.* High fat diet causes renal fibrosis in LDLr-null mice through MAPK-

755 NF-kappaB pathway mediated by Ox-LDL. *J Cardiovasc Pharmacol* **63**, 158-166
756 (2014). https://doi.org/10.1097/FJC.0000000000000035
757 7 Deng, S., Jin, T., Zhang, L., Bu, H. & Zhang, P. Mechanism of tacrolimus-induced
758 chronic renal fibrosis following transplantation is regulated by ox-LDL and its
759 receptor, LOX-1. *Mol Med Rep* **14**, 4124-4134 (2016).
760 https://doi.org/10.3892/mmr.2016.5735
761 8 Gai, Z. *et al.* Lipid Accumulation and Chronic Kidney Disease. *Nutrients* **11**
762 (2019). https://doi.org/10.3390/nu11040722
763 9 Nagase, M. *et al.* Expression of LOX-1, an oxidized low-density lipoprotein
764 receptor, in experimental hypertensive glomerulosclerosis. *J Am Soc Nephrol* **11**,
765 1826-1836 (2000). https://doi.org/10.1681/ASN.V11101826
766 10 Lu, J. *et al.* Abrogation of lectin-like oxidized LDL receptor-1 attenuates acute
767 myocardial ischemia-induced renal dysfunction by modulating systemic and local
768 inflammation. *Kidney Int* **82**, 436-444 (2012). https://doi.org/10.1038/ki.2012.186
769 11 Manttari, M., Tiula, E., Alikoski, T. & Manninen, V. Effects of hypertension and
770 dyslipidemia on the decline in renal function. *Hypertension* **26**, 670-675 (1995).
771 https://doi.org/10.1161/01.hyp.26.4.670
772 12 Brewster, U. C. & Perazella, M. A. The renin-angiotensin-aldosterone system and

773 the kidney: effects on kidney disease. *Am J Med* **116**, 263-272 (2004).
774 https://doi.org/10.1016/j.amjmed.2003.09.034
775 13 Yamamoto, K. *et al.* Oxidized LDL (oxLDL) activates the angiotensin II type 1
776 receptor by binding to the lectin-like oxLDL receptor. *FASEB J* **29**, 3342-3356
777 (2015). https://doi.org/10.1096/fj.15-271627
778 14 Takahashi, T. *et al.* The endocytosis of oxidized LDL via the activation of the
779 angiotensin II type 1 receptor. *iScience* **24**, 102076 (2021).
780 https://doi.org/10.1016/j.isci.2021.102076
781 15 Wingler, L. M. *et al.* Angiotensin Analogs with Divergent Bias Stabilize Distinct
782 Receptor Conformations. *Cell* **176**, 468-478 e411 (2019).
783 https://doi.org/10.1016/j.cell.2018.12.005
784 16 Namkung, Y. *et al.* Functional selectivity profiling of the angiotensin II type 1
785 receptor using pathway-wide BRET signaling sensors. *Sci Signal* **11** (2018).
786 https://doi.org/10.1126/scisignal.aat1631
787 17 Jono, T. *et al.* Lectin-like oxidized low density lipoprotein receptor-1 (LOX-1)
788 serves as an endothelial receptor for advanced glycation end products (AGE).
789 *FEBS Lett* **511**, 170-174 (2002). https://doi.org/10.1016/s0014-5793(01)03325-7
790 18 Lymperopoulos, A., Borges, J. I., Carbone, A. M., Cora, N. & Sizova, A.

791 Cardiovascular angiotensin II type 1 receptor biased signaling: Focus on non-Gq-,
792 non-betaarrestin-dependent signaling. *Pharmacol Res* **174**, 105943 (2021).
793 https://doi.org/10.1016/j.phrs.2021.105943
794 19 Huang, Y., Takahashi, T., Gaisano, H., Rakugi, H. & Yamamoto, K. A live-
795 imaging protocol for tracking receptor dynamics in single cells. *STAR Protoc* **3**,
796 101347 (2022). https://doi.org/10.1016/j.xpro.2022.101347
797 20 Devost, D. *et al.* Conformational Profiling of the AT1 Angiotensin II Receptor
798 Reflects Biased Agonism, G Protein Coupling, and Cellular Context. *J Biol Chem*
799 **292**, 5443-5456 (2017). https://doi.org/10.1074/jbc.M116.763854
800 21 Kobori, H. *et al.* Urinary angiotensinogen as a novel biomarker of the intrarenal
801 renin-angiotensin system status in hypertensive patients. *Hypertension* **53**, 344-
802 350 (2009). https://doi.org/10.1161/HYPERTENSIONAHA.108.123802
803 22 Jennings, B. L. *et al.* Cytochrome P450 1B1 contributes to renal dysfunction and
804 damage caused by angiotensin II in mice. *Hypertension* **59**, 348-354 (2012).
805 https://doi.org/10.1161/HYPERTENSIONAHA.111.183301
806 23 Wolak, T. *et al.* Osteopontin modulates angiotensin II-induced inflammation,
807 oxidative stress, and fibrosis of the kidney. *Kidney Int* **76**, 32-43 (2009).
808 https://doi.org/10.1038/ki.2009.90

809 24 Hu, C. *et al.* Modulation of angiotensin II-mediated hypertension and cardiac
810 remodeling by lectin-like oxidized low-density lipoprotein receptor-1 deletion.
811 *Hypertension* **52**, 556-562 (2008).
812 https://doi.org/10.1161/HYPERTENSIONAHA.108.115287
813 25 Ohki, I. *et al.* Crystal structure of human lectin-like, oxidized low-density
814 lipoprotein receptor 1 ligand binding domain and its ligand recognition mode to
815 OxLDL. *Structure* **13**, 905-917 (2005). https://doi.org/10.1016/j.str.2005.03.016
816 26 Wright, A. K. & Thompson, M. R. Hydrodynamic structure of bovine serum
817 albumin determined by transient electric birefringence. *Biophys J* **15**, 137-141
818 (1975). https://doi.org/10.1016/s0006-3495(75)85797-3
819 27 Kriz, W., Kaissling, B. & Le Hir, M. Epithelial-mesenchymal transition (EMT) in
820 kidney fibrosis: fact or fantasy? *J Clin Invest* **121**, 468-474 (2011).
821 https://doi.org/10.1172/jci44595
822 28 Jiang, T. *et al.* Diet-induced obesity in C57BL/6J mice causes increased renal lipid
823 accumulation and glomerulosclerosis via a sterol regulatory element-binding
824 protein-1c-dependent pathway. *J Biol Chem* **280**, 32317-32325 (2005).
825 https://doi.org/10.1074/jbc.M500801200
826 29 Kume, S. *et al.* Role of altered renal lipid metabolism in the development of renal

827 injury induced by a high-fat diet. *J Am Soc Nephrol* **18**, 2715-2723 (2007).
828 https://doi.org/10.1681/ASN.2007010089
829 30 Yamamoto, T. *et al.* High-Fat Diet-Induced Lysosomal Dysfunction and Impaired
830 Autophagic Flux Contribute to Lipotoxicity in the Kidney. *J Am Soc Nephrol* **28**,
831 1534-1551 (2017). https://doi.org/10.1681/ASN.2016070731
832 31 Sun, Y. *et al.* High-fat diet promotes renal injury by inducing oxidative stress and
833 mitochondrial dysfunction. *Cell Death Dis* **11**, 914 (2020).
834 https://doi.org/10.1038/s41419-020-03122-4
835 32 Yu, Y., Mo, H., Zhuo, H., Yu, C. & Liu, Y. High Fat Diet Induces Kidney Injury
836 via Stimulating Wnt/beta-Catenin Signaling. *Front Med (Lausanne)* **9**, 851618
837 (2022). https://doi.org/10.3389/fmed.2022.851618
838 33 Sato, Y. *et al.* Determination of LOX-1-ligand activity in mouse plasma with a
839 chicken monoclonal antibody for ApoB. *Atherosclerosis* **200**, 303-309 (2008).
840 https://doi.org/10.1016/j.atherosclerosis.2008.02.001
841 34 Garcia-Carro, C. *et al.* A Nephrologist Perspective on Obesity: From Kidney
842 Injury to Clinical Management. *Front Med (Lausanne)* **8**, 655871 (2021).
843 https://doi.org/10.3389/fmed.2021.655871
844 35 Tsuboi, N., Okabayashi, Y., Shimizu, A. & Yokoo, T. The Renal Pathology of

845 Obesity. *Kidney Int Rep* **2**, 251-260 (2017).
846 https://doi.org/10.1016/j.ekir.2017.01.007
847 36 Hu, C. *et al.* Deletion of LOX-1 attenuates renal injury following angiotensin II
848 infusion. *Kidney Int* **76**, 521-527 (2009). https://doi.org/10.1038/ki.2009.234
849 37 Li, X. *et al.* LOX-1 Deletion Attenuates Myocardial Fibrosis in the Aged Mice,
850 Particularly Those With Hypertension. *Front Cardiovasc Med* **8**, 736215 (2021).
851 https://doi.org/10.3389/fcvm.2021.736215
852 38 Navar, L. G., Kobori, H., Prieto, M. C. & Gonzalez-Villalobos, R. A. Intratubular
853 renin-angiotensin system in hypertension. *Hypertension* **57**, 355-362 (2011).
854 https://doi.org/10.1161/HYPERTENSIONAHA.110.163519
855 39 Navar, L. G. Translational studies on augmentation of intratubular renin-
856 angiotensin system in hypertension. *Kidney Int Suppl (2011)* **3**, 321-325 (2013).
857 https://doi.org/10.1038/kisup.2013.67
858 40 Mills, K. T. *et al.* Increased urinary excretion of angiotensinogen is associated
859 with risk of chronic kidney disease. *Nephrol Dial Transplant* **27**, 3176-3181
860 (2012). https://doi.org/10.1093/ndt/gfs011
861 41 Kidney Disease: Improving Global Outcomes Blood Pressure Work, G. KDIGO
862 2021 Clinical Practice Guideline for the Management of Blood Pressure in

863 Chronic Kidney Disease. *Kidney Int* **99**, S1-S87 (2021).
864 https://doi.org/10.1016/j.kint.2020.11.003
865 42 Yang, R., Smolders, I. & Dupont, A. G. Blood pressure and renal hemodynamic
866 effects of angiotensin fragments. *Hypertens Res* **34**, 674-683 (2011).
867 https://doi.org/10.1038/hr.2011.24
868 43 Balzer, M. S., Rohacs, T. & Susztak, K. How Many Cell Types Are in the Kidney
869 and What Do They Do? *Annu Rev Physiol* **84**, 507-531 (2022).
870 https://doi.org/10.1146/annurev-physiol-052521-121841
871 44 Mehta, J. L. *et al.* Deletion of LOX-1 reduces atherogenesis in LDLR knockout
872 mice fed high cholesterol diet. *Circ Res* **100**, 1634-1642 (2007).
873 https://doi.org/10.1161/CIRCRESAHA.107.149724
874
875
876
877
878
879
880
881

882 ## Figure Legends

883 **Fig. 1| Oxidized LDL potentiates Ang II-induced Gq signaling and calcium influx in**

884 **a LOX-1-dependent manner**

885 **a** Dose-dependent response of IP1 concentration by the activation of Gq signaling in

886 response to oxLDL and Ang II in CHO-LOX-1-AT1 cells. Cells were treated with oxLDL

887 and Ang II at the concentrations described in the figure. (n=4 for each oxLDL

888 concentration). $^{*}P$=0.0004 for 0 μg/mL vs 20 μg/mL, $^{\dagger}P$=0.0003 for 5 g/mL vs 20 μg/mL,

889 ‡P=0.0020 for 0 μg/mL vs 10 μg/mL, and $^{\S}P$=0.0015 for 5 μg/mL vs 10 μg/mL at 10^{-9} M

890 Ang II; $^{\parallel}P$=0.0051 for 0 μg/mL vs 10 μg/mL, $^{\P}P$=0.0004 for 0 μg/mL vs 20 μg/mL at 10^{-}

891 ^{8} M Ang II.

892 **b** IP1 concentration in response to vehicle, native LDL (nLDL 10 μg/mL), and oxLDL

893 (10 μg/mL) in the combination of Ang II (10^{-8} M) in CHO-LOX-1-AT1 cells (n=5 for

894 each group)

895 **c** IP1 concentration in response to vehicle, oxLDL (10 μg/mL) in the combination of Ang

896 II (10^{-8}M) in CHO-LOX-1-AT1 and CHO-AT1 cells (n=5 for each group).

897 **d** IP1 concentration in response to vehicle, oxLDL (10 μg/mL), BSA (10 or 100 μg/mL),

898 BSA-conjugated AGE (10 or 100 μg/mL) in the combination of Ang ll (10^{-8} M) in CHO-

899 LOX-1-AT1 cells.

900 **e** IP1 concentration in response to vehicle, oxLDL (10 μg/mL) in the combination of Ang
901 II (10^{-8} M) in genetically engineered CHO cells with or without intact β-arrestin binding
902 domain (n=5 for each group). AT1mg indicates AT1 a mutant AT1 lacking a functional β-
903 arrestin binding domain but retaining G-protein-biased signaling capability.
904 **f** IP1 concentration in response to oxLDL (10 μg/mL) in the combination of Ang II (10^{-8}
905 M) and additional effect of PTX, a Gi inhibitor, YM-254890, a Gq inhibitor, and RKI-
906 1448, a downstream Rho kinase inhibitor targeting G12/13 signaling, in CHO-LOX-1-
907 AT1 cells (n=5 for each group).
908 **g** Intracellular calcium dynamics measured using Fura 2-AM by the ratio of the mission
909 signals at excitation wavelength 340 nm and 380 nm in response to oxLDL (5 μg/mL),
910 Ang II (10^{-12} M), and their combination (for each agonist, 4-7 regions of interest were
911 selected). Addition of these agonists is marked with arrows on the timeline of the assay.
912 **h** Percentage changes from baseline in the ratio of emission signals (F340/F380)
913 measured by Fura 2-AM were quantified following treatment with oxLDL and Ang II at
914 specified concentrations in CHO-LOX-1-AT1 cells as detailed in the figure (n=4-8).
915 **i** Percentage change from baseline in the ratio of emission signals (F340/F380) measured
916 by Fura 2-AM after stimulation with oxLDL (5 μg/mL), Ang II (10^{-12} M), and YM-
917 254890, a Gq inhibitor, in CHO-LOX-1-AT1 cells.

918 **j** Percentage changes from baseline in the ratio of emission signals (F340/F380) measured

919 by Fura 2-AM were quantified following treatment with oxLDL (5 μg/mL) and Ang II at

920 specified concentrations in CHO-AT1 cells, as detailed in the figure.

921 Data are represented as mean ± SEM. Differences were determined using one-way

922 ANOVA, followed by Tukey's multiple comparison test for (a-f) and (h-j).

923

924 **Fig. 2| Co-treatment of oxLDL with Ang II induces conformational change of AT1**

925 **different from each treatment alone**

926 **a** Change in green puncta (AT1-eGFP) and red puncta (LOX-1-mScarlet) by the treatment

927 with vehicle, oxLDL (10μg/mL), Ang II (10^{-5}M), and the combination of oxLDL and Ang

928 II in CHO cell overexpressing these fluorescent protein-conjugated receptors (n=10-11

929 for each group). The puncta were manually counted by a blinded observer and the number

930 of puncta at 0 and 3 min was determined (N0 and N3, respectively). The change in puncta

931 was calculated as (N0-N3)/N0.

932 **b-d** Changes in BRET signals were monitored in CHO-LOX-1 cells expressing the

933 following conformational biosensors: AT1-C-tailP1 (b) and AT1-ICL3P3 (c, d) bearing

934 FlAsH insertion at the cytoplasmic-terminal tail (C-tailP1) and the third intracellular loop

935 (ICL3P3) of AT1, respectively, that interact with Renilla luciferase at the end of the

936 cytoplasmic tail. Cells were subjected to treatments with vehicle, oxLDL (10 μg/mL),
937 Ang II (10^{-5}M), the combination of Ang II and oxLDL, and the combination
938 of AngII, oxLDL and LOX-1 antibody. The BRET ratios were calculated every 16
939 seconds for a total of 320 seconds and the relative change in intramolecular BRET ratio
940 (ΔBRET) was calculated by subtracting the average BRET ratio measured for cells
941 stimulated with vehicle at each time point. Lower panels indicate average ΔBRET of all
942 the time points during measurement.
943 Data are represented as mean ± SEM. Differences were determined by one-way ANOVA,
944 followed by Tukey's multiple comparison test (a-d).
945
946 **Fig. 3| Oxidized LDL potentiates Ang II-induced Gq-calcium signaling in renal cells**
947 **a, b** IP1 concentration in response to Ang II (10^{-7} M), oxLDL (10 μg/mL), and the
948 combination of both with or without YM-254890, Gq inhibitor, in NRK52E (a) and
949 NRK49F cells (b) (n=5 for each group).
950 **c, d** IP1 concentration in response to Ang II (10^{-7} M) and oxLDL (10 μg/mL) in the
951 combination of Ang II (10^{-7} M) and the additional effect of siRNA-mediated knockdown
952 of *AT1a* or *LOX-1* in NRK52E (c) and NRK49F cells (d) (n=5 for each group).
953 **e** Intracellular calcium concentration in NRK49F cells using Fura 2-AM and dual-

954 excitation microfluorometry. Changes in the fluorescence intensity ratio (F340/F380)
955 served as an index of the calcium dynamics. Cells were exposed to Ang II (10^{-7} M),
956 oxLDL (2 μg/mL), and a combination of both agents. Addition of these agonists is marked
957 with arrows on the timeline of the assay. Data acquisition and analysis were performed
958 using a digital image analyzer to monitor real-time calcium flux (n=4-9).
959 **f** Percentage changes from baseline in the ratio of emission signals (F340/F380) measured
960 by Fura 2-AM were quantified following treatment with Ang II (10^{-7} M) and oxLDL at
961 the concentrations detailed in the figure in NRK49F cells (n=5 for each group).
962 **g** Impact of siRNA-mediated knockdown *AT1* or *LOX-1* on the percentage changes from
963 baseline in the ratio of emission signals (F340/F380) measured by Fura 2-AM were
964 quantified following treatment with Ang II (10^{-7} M) and oxLDL (2 μg/mL) in NRK49F
965 cells (n=3-7).
966 **g** Impact of co-treatment of YM-254890, Gq inhibitor, or Irbesartan, an angiotensin
967 receptor blocker (ARB), on the the percentage changes from baseline in the ratio of
968 emission signals (F340/F380) measured by Fura 2-AM were quantified following
969 treatment with Ang II (10^{-7} M) and oxLDL (2 μg/mL) in NRK49F cells (n=4 for each
970 group).
971 Data are represented as mean ± SEM. Differences were determined using one-way

ANOVA, followed by Tukey's multiple comparison test for (a-d) and (f-h).

Fig. 4| Co-treatment of oxLDL and AII enhanced cellular response upon Gq activation in renal cells

a,b Quantitative real-time PCR analysis was performed to measure the gene expression of NADPH oxidase subunits (*p67phox* and *p91phox*), fibrosis markers (*fibronectin*, *collagen-1*, *collagen-4*, and *TGFβ*), and inflammatory cytokines (*TNFα*, *IL1β*, *IL-6*, and *MCP-1*) in NRK49F cells (a) and NRK 52E cells (b). Gene expression levels were normalized to those of GAPDH. Cells were stimulated by oxLDL (5 μg/mL), Ang II (10^{-7} M) or their combination (n=4 for each group).

c, d Cells were pre-treated with vehicle or Gq inhibitor (YM-254890, Gqi), followed by treatment with vehicle or the combination of oxLDL (5 μg/mL) and Ang II (10^{-7} M) in NRK49F cells (c) and NRK 52E cells (d) (n=4 for each group).

e, f Cells were pre-treated with vehicle or ARB (Irbesartan, Arb), followed by treatment with vehicle or the combination of oxLDL (5 μg/mL) and Ang II (10^{-7} M) in NRK49F cells (e) and NRK 52E cells (f) (n=4 for each group).

Data are represented as mean ± SEM. Differences were determined by one-way ANOVA, followed by Tukey's multiple comparison test (a-f).

990

991 **Fig. 5| Oxidized LDL enhanced Ang II-induced epithelial mesenchymal transition in**

992 **NRK52E and NRK49F cells**

993 **a, b** Left: Western blot analysis of α-smooth muscle actin (α-SMA), a marker of

994 epithelial–mesenchymal transition (EMT), in NRK49F (a) and NRK52E (b) cells. Cells

995 were stimulated with oxLDL (5 μg/mL), Ang II (10^{-7} M), and TGF-β (10 ng/mL), with

996 TGF-β serving as a well-known EMT inducer. Right: Densitometric analysis of α-SMA

997 protein expression normalized to α-Tubulin (n=3 for each group).

998 **c, d** Left: Western blot analysis of α-SMA in NRK49F (c) or NRK52E (d) after stimulation

999 with oxLDL (5 μg/mL), Ang II (10^{-7} M), and their combination. Right: Densitometric

1000 analysis of α-SMA protein expression normalized to α-tubulin (n=3 for each group).

1001 **e, f** Left: Western blot analysis of α-SMA in NRK49F(e) or NRK52E (f) after treatment

1002 with a combination of oxLDL (5 μg/mL) and Ang II (10^{-7} M). Prior to this treatment, the

1003 cells were pre-treated with either a vehicle or a Gq inhibitor (YM-254890, Gqi). Right:

1004 Densitometric analysis of α-SMA protein expression normalized to α-Tubulin (n=3 for

1005 each group).

1006 **g, h** Left: Western blot analysis of α-SMA in NRK49F (e) or NRK52E (f) after treatment

1007 with a combination of oxLDL (5 μg/mL) and Ang II (10^{-7} M). Prior to treatment, cells

1008 were pre-treated with either vehicle or ARB (Irbesartan, Arb). Right: Densitometric

1009 analysis of α-SMA protein expression normalized to α-tubulin (n=3 for each group).

1010 Data are represented as mean ± SEM. Differences were determined by one-way ANOVA,

1011 followed by Tukey's multiple comparison test (a-f).

1012

1013 **Fig. 6| Oxidized LDL enhanced Ang II-induced renal fibroblast proliferation via**

1014 **AT1-Gq signaling and LOX-1-dependent manner**

1015 **a** Proliferative activity assessed by BrdU incorporation into NRK49F cells. Cells were

1016 pretreated with vehicle, YM-254890, or ARB, Irbesartan, followed by the treatment with

1017 oxLDL (5 μg/mL), Ang II (10^{-7} M), or their combination. (n=5 for each group).

1018 **b** NRK49F cells were subjected to siRNA-mediated knockdown using specific siRNAs

1019 for *AT1a* (siAT1) or *LOX-1* (siLOX-1). Following knockdown, cells were treated with

1020 either vehicle, oxLDL (5 μg/mL), Ang II (10^{-7} M), or their combination. Proliferative

1021 activity was assessed by measuring the BrdU levels (n=5 for each group).

1022 Data are represented as mean ± SEM. Differences were determined using one-way

1023 ANOVA, followed by Tukey's multiple comparison test for (a) and (b).

1024

1025 **Fig. 7| Oxidized LDL-inducible diet exacerbates Ang II-induced renal dysfuntion in**

1026 **wildtype mice, but not in LOX-1 knockout mice**

1027 **a** A Schematic protocol for the animal experiments. Eight-week-old male WT mice and

1028 male LOX-1 KO mice were fed either an ND or an HFD for 6 weeks. After 10 weeks of

1029 age, the mice were treated over a 4-week period with infusions of either saline or Ang II.

1030 Ang II was administered at two dosage levels: a subpressor dose of 0.1 γ and a pressor

1031 dose of 0.7 γ, delivered via subcutaneously implanted osmotic pumps. At the end of the

1032 infusion period, urine was collected, the animals were sacrificed, and comprehensive

1033 tissue analysis was conducted to evaluate the renal effects of the treatments.

1034 **b** Average systolic blood pressure (SBP) measured at half-week intervals in WT and

1035 LOX-1 KO mice during the 4-week infusion period.

1036 **c, d** Urine 8-OHDG concentrations (mg/g creatinine [Cr]) (c) and urine albumin

1037 concentrations (mg/g creatinine [Cr]) (d) in WT and LOX-1 KO mice at the conclusion

1038 of the 4-week infusion period.

1039 Data are represented as mean ± SEM. Differences were determined by one-way ANOVA,

1040 followed by Tukey's multiple comparison test (a-d).

1041

1042

1043 **Fig. 8| A high-fat diet enhanced Ang II-induced renal injury-related gene expression**

1044 **in the kidney in a LOX-1-dependent manner.**

1045 Quantitative real-time PCR analysis for gene expression of NADPH components

1046 (*p67phox and p91phox*), inflammatory cytokines (*IL-6, TNFα, IL1β, and MCP-1*), and

1047 fibrosis markers (*TGFβ, fibronectin, collagen-1a, and collagen-4a*) in the kidney

1048 harvested from WT and LOX-1 KO mice.

1049 The experimental procedures, including the dietary regimen and Ang II administration,

1050 are detailed in Fig. 7a.

1051 Data are represented as mean ± SEM. Differences were determined using one-way

1052 ANOVA, followed by Tukey's multiple comparison test for (a) and (b).

1053

1054 **Fig. 9| LOX-1 and AT1a were predominantly co-localized in renal tubules**

1055 **a, b** Representative images depicting staining for LOX-1 (a) and AT1 (b) in the renal

1056 cortex tissues from wildtype mice (WT) and LOX-1 knockout mice (LOX-1 KO). Nuclei

1057 are stained blue with DAPI. Green and red signals indicates AT1, while the red signal

1058 indicates LOX-1. Overlay images demonstrate the merged visualization of AT1 or LOX-

1059 1 with DAPI, highlighting the predominant colocalization of LOX-1 and AT1 in renal

1060 tubules as opposed to the glomerulus.

1061

1062 **Fig. 10| Schematic overview of the AT1 and LOX-1 Interaction dynamics in renal**

1063 **cells**

1064 This schematic summary illustrates the predicted structure-activation relationship of the

1065 AT1 receptor within the LOX-1-AT1 complex in renal component cells. This highlights

1066 how the simultaneous binding of Ang II to AT1 and oxLDL to LOX-1 induces

1067 conformational changes in AT1. These changes were more pronounced than those

1068 triggered by the individual ligands. Such structural alterations have been proposed to

1069 amplify Gq signaling pathway activation, subsequently leading to renal damage.

1070

1071

1072

1073

1074

1075

1076

1077

1078

1079

1080 ## Supplemental Figure Legends

1081 **Fig. S1| Live-imaging analysis of membrane LOX-1 and AT1 in response to the co-**

1082 **treatment of oxLDL with AngII.**

1083 Real-time membrane imaging of CHO cells co-transfected with LOX-1-mScarlet and

1084 AT1-eGFP in response to oxLDL (10μg/ml) in the combination of Ang II (10^{-7}M)

1085 (Supplemental Video). A count of puncta was performed using separate images

1086 visualizing LOX-1-mScarlet (red puncta) and AT1-eGFP (green puncta) immediately

1087 before and 3 min after ligand application.

1088

1089 **Fig. S2| Oxidized LDL in combination with Ang II do not increase cellular IP1**

1090 **content in human umbilical vein endothelial cells and bovine vascular endothelial**

1091 **cells, human aortic vascular smooth muscle cells, and rat macrophages**

1092 IP1 concentration in response to oxLDL (10μg/ml) in the combination of Ang II (10^{-7}M)

1093 in HUVECs (human umbilical vein endothelial cell), BAECs (bovine aortic endothelial

1094 cell), HAVSMCs (human aortic vascular smooth muscle cell), and A10 cells (rat

1095 macrophages).

1096 Data are represented as mean ± SEM. Differences were determined using one-way

1097 ANOVA, followed by Tukey's multiple comparison test (n=5 for each group).

1098

1099 **Fig. S3| Efficiency of siRNA-mediated knockdown for *AT1a* and *LOX-1* in NRK52E**

1100 **and NRK49F cells**

1101 NRK52E and NRK49F cells were transfected with siRNAs against scrambled siRNA,

1102 *AT1a* or *LOX-1*. The efficiency of siRNA-mediated gene silencing was quantified by

1103 assessing *AT1a* and *LOX-1* expression levels using quantitative real-time PCR.

1104 Data are represented as mean ± SEM. Differences were determined using one-way

1105 ANOVA, followed by Tukey's multiple comparison test.

1106

1107 **Fig. S4| Calcium influx was not induced by either the combination treatment of Ang**

1108 **II or oxLDL or each treatment alone in NRK52E cells**

1109 Percentage changes from baseline in the ratio of emission signals (F340/F380) measured

1110 by Fura 2-AM were quantified following treatment with Ang II (10^{-7}M) and oxLDL at

1111 the concentrations detailed in the figure for NRK49E cells (n=5-7 for each group).

1112 Data are represented as mean ± SEM. Differences were determined using one-way

1113 ANOVA, followed by Tukey's multiple comparison test.

1114

1115 **Fig. S5| High Fat Diet used in the study prominently increased plasma LOX-1 ligand**

1116 **concentration**

1117 Plasma LOX-1 ligand concentration of 14-week-old wildtype mice upon ND and HFD

1118 for 6 weeks. From 10 weeks of age, these mice also received concurrent 4-week infusions

1119 of Ang II at a pressor dose of 0.7 γ, administered through subcutaneously implanted

1120 osmotic pumps.

1121 Data are represented as mean ± SEM. Differences were determined using Student's t-test

1122 (n=7 for each group).

1123

1124 **Fig. S6 | Impact of Diet and Ang II Infusion on Body Weight and Systolic Blood**

1125 **Pressure in Mice**

1126 **a** Final Body weight: This figure shows the body weights of WT and LOX-1 KO mice at

1127 the end of the 4-week infusion period, highlighting the effects of diet and pharmacological

1128 treatment.

1129 **b, c** Serial Body Weight Changes: These graphs depict the progression of body weight

1130 over time in WT and LOX-1 KO mice, illustrating the impact of the dietary regimen and

1131 Ang II infusion on weight dynamics.

1132 **d, e** Systolic Blood Pressure Trajectory: Serial measurements of systolic blood pressure

1133 (SBP) obtained using the tail-cuff method are presented for WT and LOX-1 KO mice.

1134 The figures show the changes in SBP over the course of the study, corresponding to the

1135 administration of a pressor dose of 0.7 γ (d) and a subpressor dose of 0.1 γ (e) of Ang II,

1136 respectively.

1137 **f** Final SBP: This figure shows SBP of WT and LOX-1 KO mice at the end of the 4-week

1138 infusion period, highlighting the effects of diet and pharmacological treatments.

1139 Beginning at 8 weeks of age, mice were fed either an ND or an HFD for 6 weeks. From

1140 10 weeks of age, coinciding with the 2-week time point in the figure, the rats underwent

1141 a 4-week period of infusion with either vehicle or Ang II. The infusion was delivered at

1142 specific dosage levels through subcutaneously implanted osmotic pumps.

1143 Data are represented as mean ± SEM. Differences were determined using one-way

1144 ANOVA, followed by Tukey's multiple comparison test for (a) and (b).

1145

1146 **Fig. S7| No significant difference was found in plasma aldosterone concentration**

1147 **between a normal diet and a high fat diet-fed wildtype mice with a pressor dose of**

1148 **Ang II**

1149 Plasma aldosterone concentration in 14-week-old wild-type mice fed an ND or an HFD

1150 for 6 weeks. From 10 weeks of age, these mice also received concurrent 4-week infusions

1151 of Ang II at a pressor dose of 0.7 γ, administered through subcutaneously implanted

1152 osmotic pumps.

1153 Data are represented as mean ± SEM. Differences were determined using Student's t-test

1154 (n=7 for each group).

1155

1156 **Fig. S8| A high-fat diet enhanced Ang II-induced renal injury-related gene**

1157 **expression in the kidney in a LOX-1-dependent manner.**

1158 Quantitative real-time PCR analysis for gene expression of NADPH components

1159 (*p40phox and p47phox*), inflammatory gene (*COX-2*), fibrosis markers (*αSMA and*

1160 *vimentin*), epithelial markers (*E-cadherin and cadherin-16*), tubular marker (*NAGL*),

1161 *AT1a*, *AT1b*, and *LOX-1* in the kidney harvested from WT and LOX-1 KO mice.

1162 The experimental procedures, including the dietary regimen and Ang II administration,

1163 are detailed in Fig. 7a.

1164 Data are represented as mean ± SEM. Differences were determined using one-way

1165 ANOVA, followed by Tukey's multiple comparison test for (a) and (b).

1166

1167 **Fig. S9| The treatment with Ang II, a High Fat Diet, or their combination for 4 weeks**

1168 **did not induce any histological changes indicative of renal injury**

1169 **a** Left: Representative histological images of Masson-Trichrome staining used to detect

1170 fibrosis in renal tissues harvested from WT and LOX-1 KO mice. Right: Quantitative

1171 analysis by Masson-Trichrome staining.

1172 Data are represented as mean ± SEM. Differences were determined using one-way

1173 ANOVA, followed by Tukey's multiple comparison test.

1174 **b** Representative histological images of renal tissues harvested from WT and LOX-1 KO

1175 mice stained for PAS to assess mesangial expansion and glomerular area, providing

1176 insight into the structural integrity of the glomeruli.

1177 Eight-week-old mice were fed an ND or an HFD for 6 weeks. From 10 weeks of age,

1178 these mice were concurrently treated for 4 weeks with infusions of vehicle or Ang II (a

1179 subpressor dose of 0.1 γ or a pressor dose of 0.7 γ) through subcutaneously implanted

1180 osmotic pomps.

1181

1182

1183

1184

1185

Fig. 1

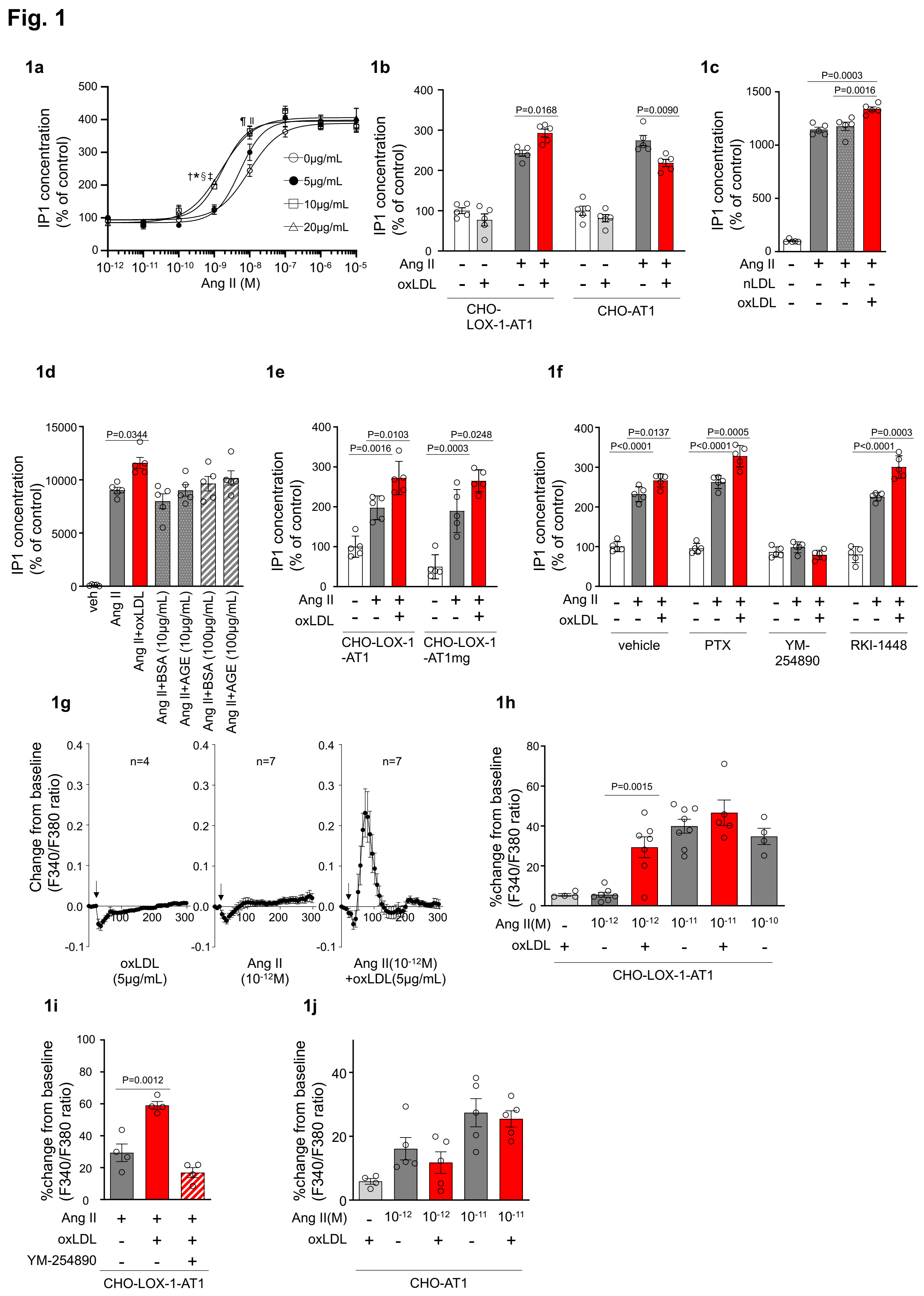
1a
IP1 concentration (% of control)
Ang II (M)
0μg/mL
5μg/mL
10μg/mL
20μg/mL
1b
P=0.0168
P=0.0090
Ang II
oxLDL
CHO-LOX-1-AT1
CHO-AT1
1c
P=0.0003
P=0.0016
Ang II
nLDL
oxLDL
1d
P=0.0344
veh
Ang II
Ang II+oxLDL
Ang II+BSA (10μg/mL)
Ang II+AGE (10μg/mL)
Ang II+BSA (100μg/mL)
Ang II+AGE (100μg/mL)
1e
P=0.0103
P=0.0016
P=0.0248
P=0.0003
CHO-LOX-1-AT1
CHO-LOX-1-AT1mg
1f
P=0.0137
P<0.0001
P=0.0005
P<0.0001
P=0.0003
P<0.0001
vehicle
PTX
YM-254890
RKI-1448
1g
n=4
n=7
n=7
Change from baseline (F340/F380 ratio)
oxLDL (5μg/mL)
Ang II (10-12M)
Ang II(10-12M) +oxLDL(5μg/mL)
1h
P=0.0015
%change from baseline (F340/F380 ratio)
Ang II(M)
oxLDL
CHO-LOX-1-AT1
1i
P=0.0012
Ang II
oxLDL
YM-254890
CHO-LOX-1-AT1
1j
Ang II(M)
oxLDL
CHO-AT1

Fig. 2

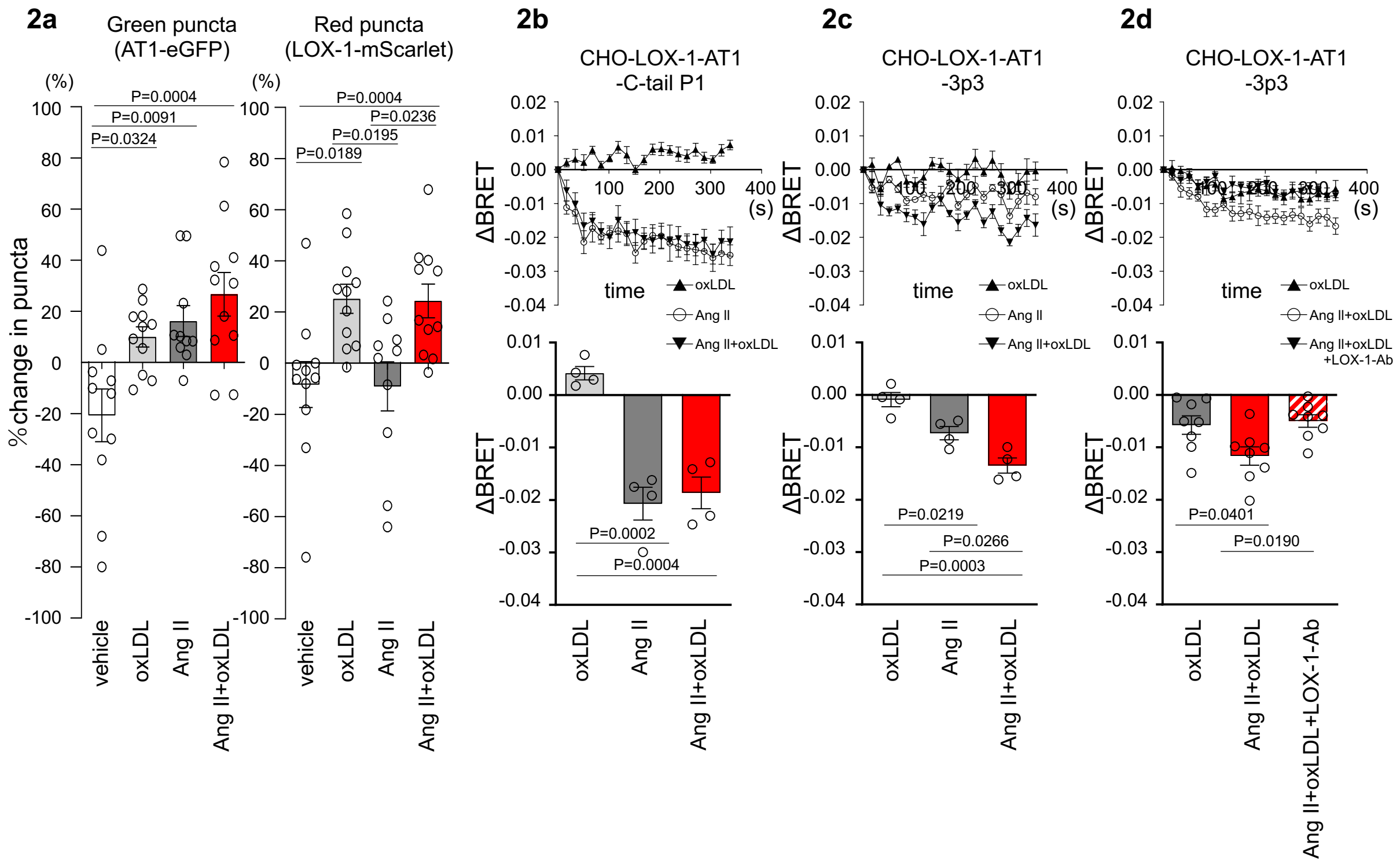
2a
Green puncta
(AT1-eGFP)
Red puncta
(LOX-1-mScarlet)
(%)
% change in puncta
P=0.0004
P=0.0091
P=0.0324
P=0.0004
P=0.0236
P=0.0195
P=0.0189
vehicle
oxLDL
Ang II
Ang II+oxLDL
2b
CHO-LOX-1-AT1
-C-tail P1
ΔBRET
time
(s)
oxLDL
Ang II
Ang II+oxLDL
P=0.0002
P=0.0004
2c
CHO-LOX-1-AT1
-3p3
P=0.0219
P=0.0266
P=0.0003
2d
CHO-LOX-1-AT1
-3p3
Ang II+oxLDL
Ang II+oxLDL
+LOX-1-Ab
P=0.0401
P=0.0190
Ang II+oxLDL+LOX-1-Ab

Fig. 3

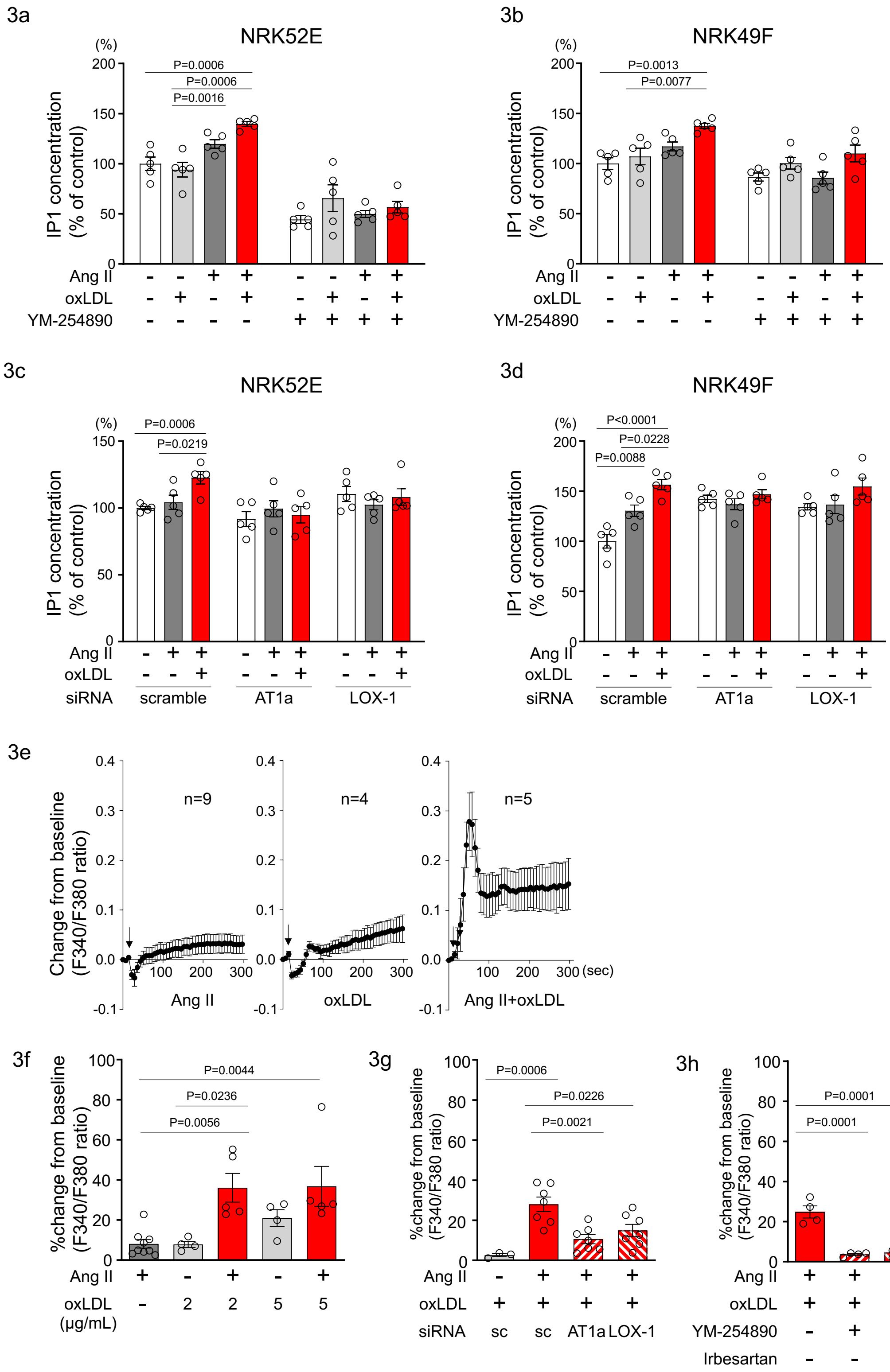
3a
NRK52E
(%)
IP1 concentration (% of control)
P=0.0006
P=0.0006
P=0.0016
Ang II
oxLDL
YM-254890
3b
NRK49F
P=0.0013
P=0.0077
3c
NRK52E
P=0.0006
P=0.0219
siRNA
scramble
AT1a
LOX-1
3d
NRK49F
P<0.0001
P=0.0228
P=0.0088
3e
Change from baseline (F340/F380 ratio)
n=9
n=4
n=5
Ang II
oxLDL
Ang II+oxLDL
(sec)
3f
%change from baseline (F340/F380 ratio)
P=0.0044
P=0.0236
P=0.0056
oxLDL (μg/mL)
3g
P=0.0006
P=0.0226
P=0.0021
sc
AT1a
LOX-1
3h
P=0.0001
P=0.0001
YM-254890
Irbesartan

Fig. 4

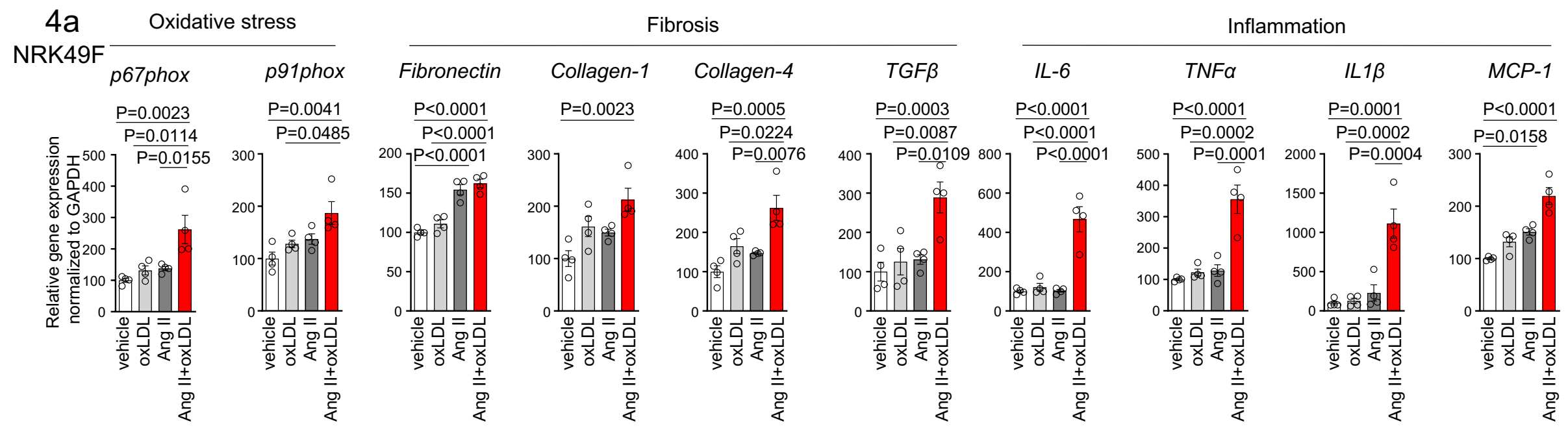
4a
NRK49F
Oxidative stress
Fibrosis
Inflammation
p67phox
p91phox
Fibronectin
Collagen-1
Collagen-4
TGFβ
IL-6
TNFα
IL1β
MCP-1
P=0.0023
P=0.0114
P=0.0155
P=0.0041
P=0.0485
P<0.0001
P<0.0001
P<0.0001
P=0.0023
P=0.0005
P=0.0224
P=0.0076
P=0.0003
P=0.0087
P=0.0109
P<0.0001
P<0.0001
P<0.0001
P<0.0001
P=0.0002
P=0.0001
P=0.0001
P=0.0002
P=0.0004
P<0.0001
P=0.0158
Relative gene expression normalized to GAPDH
vehicle
oxLDL
Ang II
Ang II+oxLDL

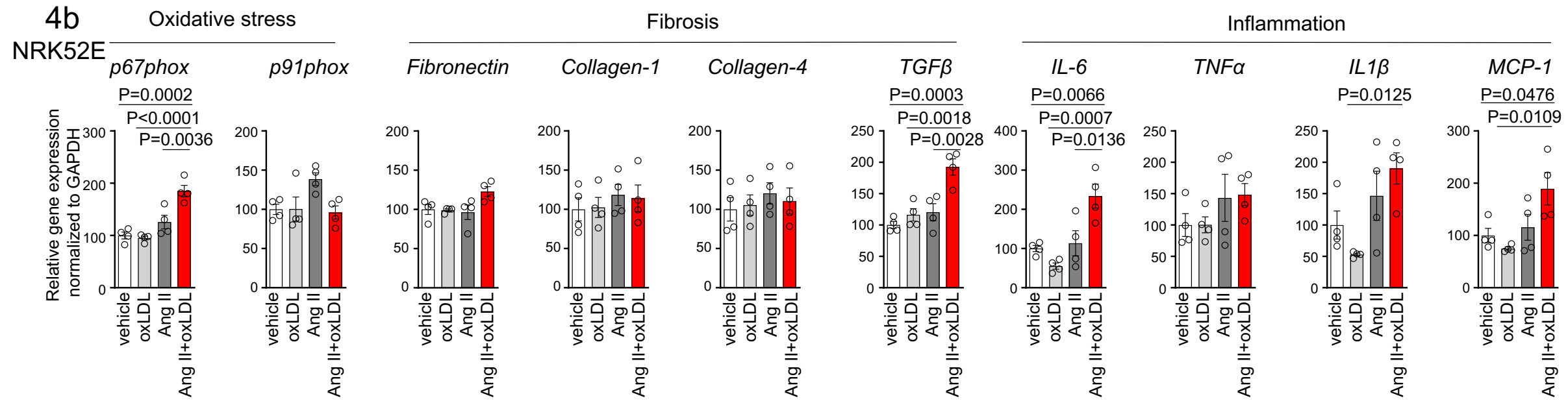
4b
NRK52E
Oxidative stress
Fibrosis
Inflammation
p67phox
p91phox
Fibronectin
Collagen-1
Collagen-4
TGFβ
IL-6
TNFα
IL1β
MCP-1
P=0.0002
P<0.0001
P=0.0036
P=0.0003
P=0.0018
P=0.0028
P=0.0066
P=0.0007
P=0.0136
P=0.0125
P=0.0476
P=0.0109
Relative gene expression normalized to GAPDH
vehicle
oxLDL
Ang II
Ang II+oxLDL

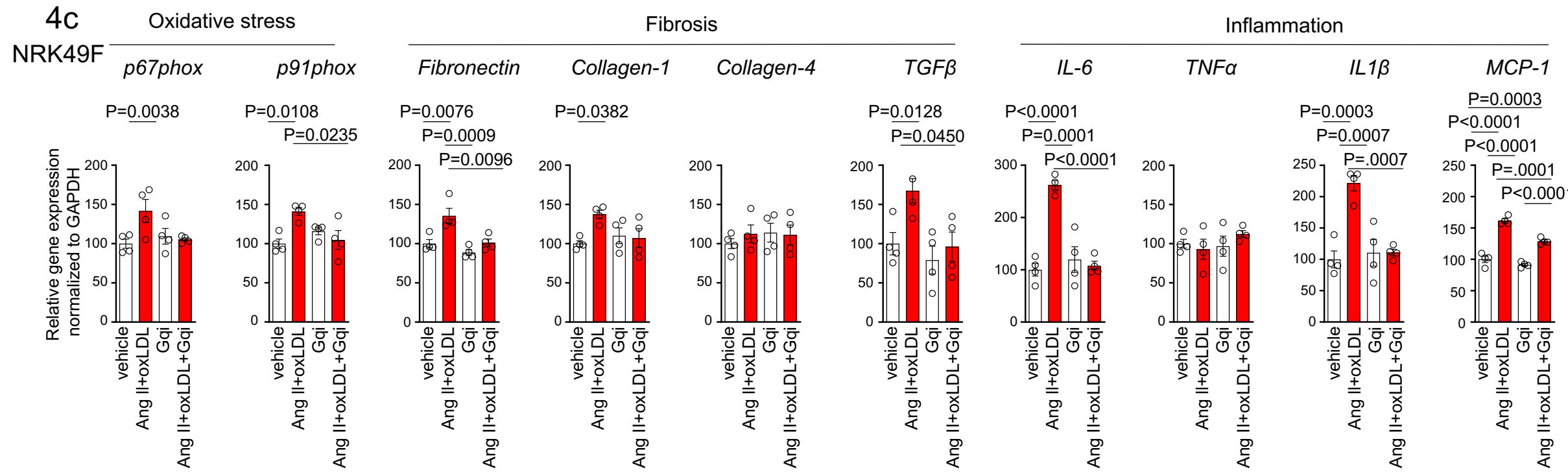
4c
NRK49F
Oxidative stress
Fibrosis
Inflammation
p67phox
p91phox
Fibronectin
Collagen-1
Collagen-4
TGFβ
IL-6
TNFα
IL1β
MCP-1
P=0.0038
P=0.0108
P=0.0235
P=0.0076
P=0.0009
P=0.0096
P=0.0382
P=0.0128
P=0.0450
P<0.0001
P=0.0001
P<0.0001
P=0.0003
P=0.0007
P=.0007
P=0.0003
P<0.0001
P<0.0001
P=.0001
P<0.0001
Relative gene expression normalized to GAPDH
vehicle
Ang II+oxLDL
Gqi
Ang II+oxLDL+Gqi

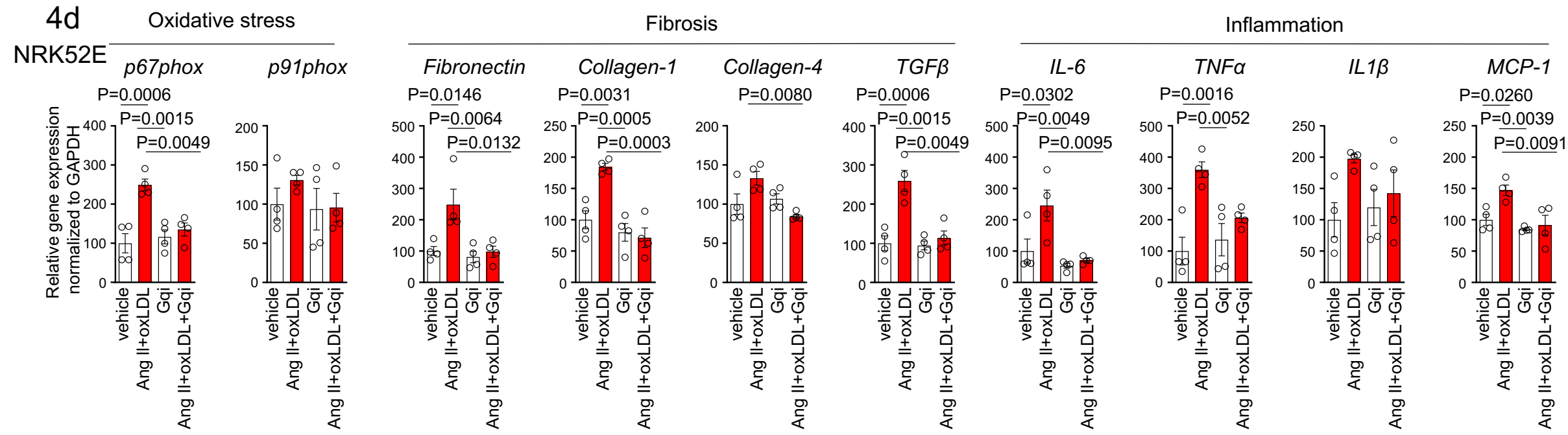
4d
NRK52E
Oxidative stress
Fibrosis
Inflammation
p67phox
p91phox
Fibronectin
Collagen-1
Collagen-4
TGFβ
IL-6
TNFα
IL1β
MCP-1
P=0.0006
P=0.0015
P=0.0049
P=0.0146
P=0.0064
P=0.0132
P=0.0031
P=0.0005
P=0.0003
P=0.0080
P=0.0006
P=0.0015
P=0.0049
P=0.0302
P=0.0049
P=0.0095
P=0.0016
P=0.0052
P=0.0260
P=0.0039
P=0.0091
Relative gene expression normalized to GAPDH
vehicle
Ang II+oxLDL
Gqi
Ang II+oxLDL+Gqi

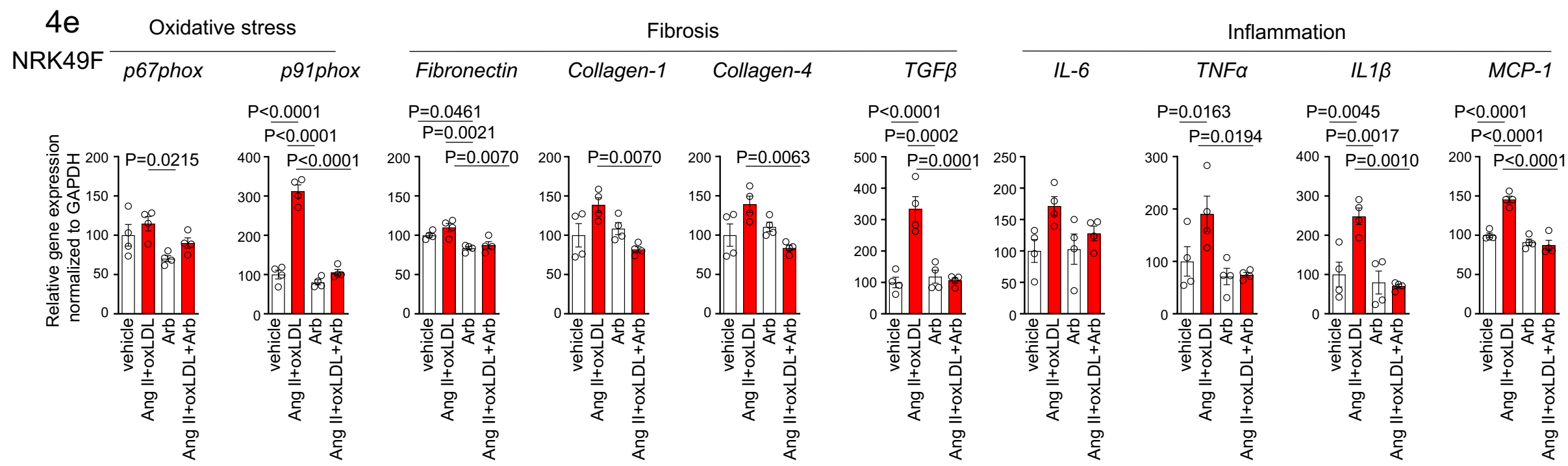
4e
NRK49F
Oxidative stress
Fibrosis
Inflammation
p67phox
p91phox
Fibronectin
Collagen-1
Collagen-4
TGFβ
IL-6
TNFα
IL1β
MCP-1
P=0.0215
P<0.0001
P<0.0001
P=0.0461
P=0.0021
P=0.0070
P=0.0070
P=0.0063
P<0.0001
P=0.0002
P=0.0001
P=0.0163
P=0.0194
P=0.0045
P=0.0017
P=0.0010
P<0.0001
P<0.0001
Relative gene expression normalized to GAPDH
vehicle
Ang II+oxLDL
Arb
Ang II+oxLDL+Arb

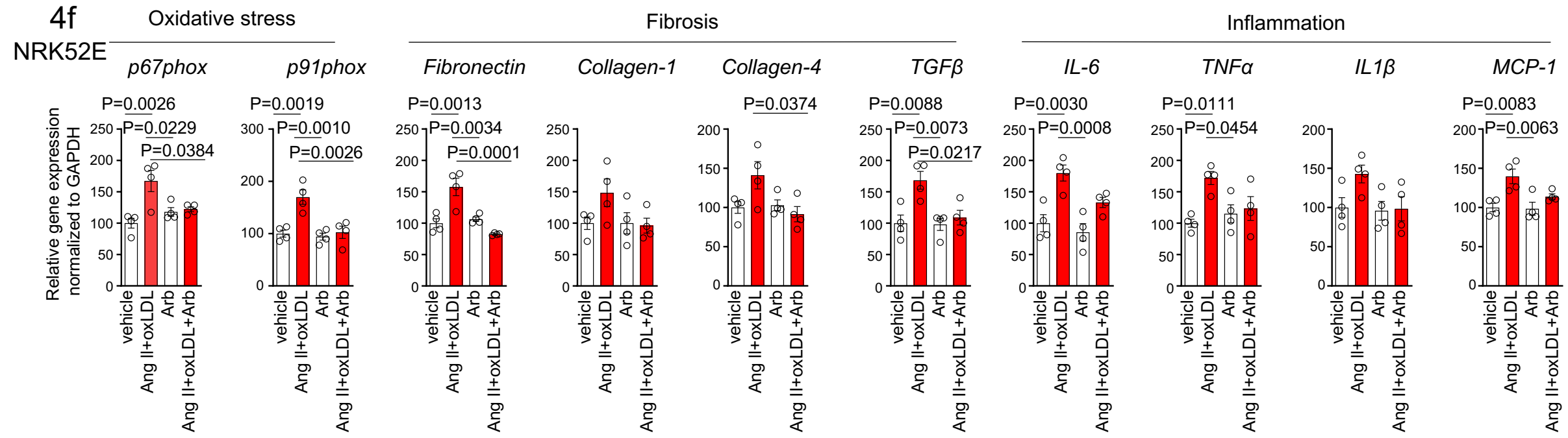
4f
NRK52E
Oxidative stress
Fibrosis
Inflammation
p67phox
p91phox
Fibronectin
Collagen-1
Collagen-4
TGFβ
IL-6
TNFα
IL1β
MCP-1
P=0.0026
P=0.0229
P=0.0384
P=0.0019
P=0.0010
P=0.0026
P=0.0013
P=0.0034
P=0.0001
P=0.0374
P=0.0088
P=0.0073
P=0.0217
P=0.0030
P=0.0008
P=0.0111
P=0.0454
P=0.0083
P=0.0063
Relative gene expression normalized to GAPDH
vehicle
Ang II+oxLDL
Arb
Ang II+oxLDL+Arb

Fig. 5

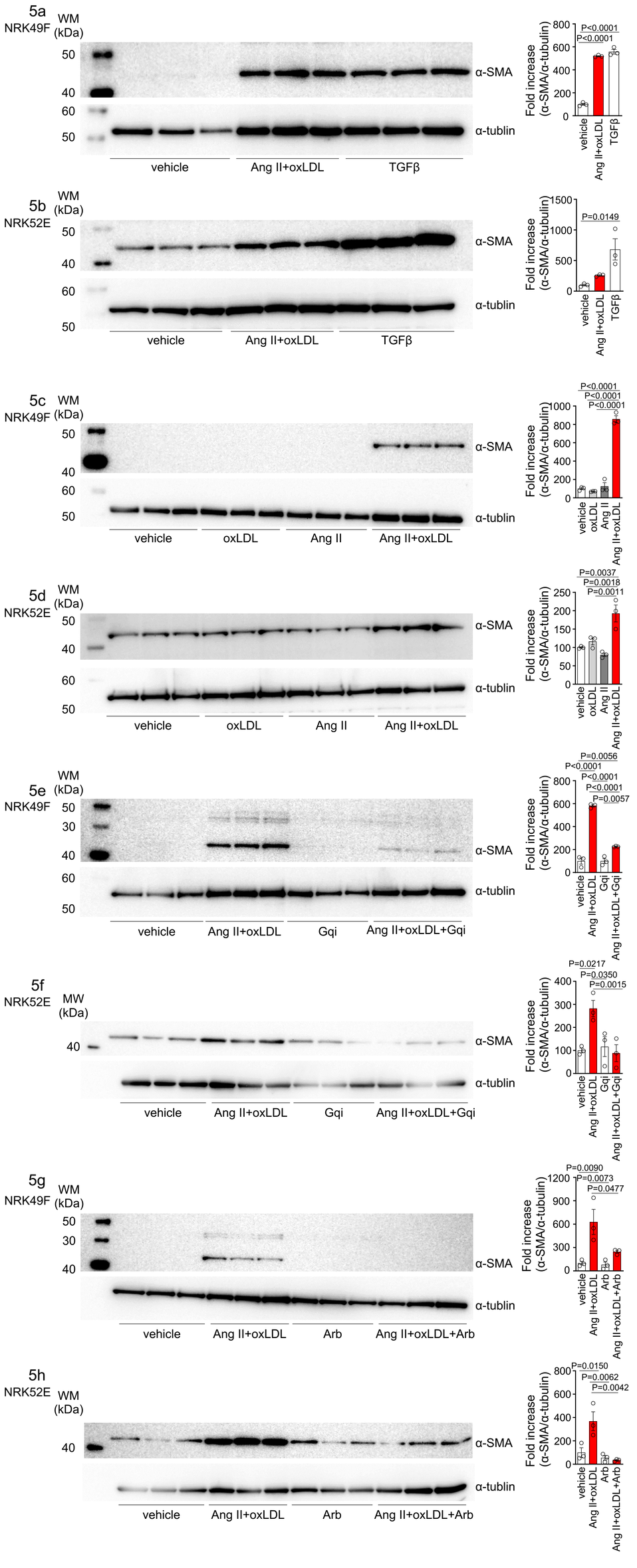
5a
NRK49F
WM (kDa)
50
40
60
50
α-SMA
α-tublin
vehicle
Ang II+oxLDL
TGFβ
Fold increase (α-SMA/α-tubulin)
P<0.0001
P<0.0001
5b
NRK52E
P=0.0149
5c
NRK49F
vehicle
oxLDL
Ang II
Ang II+oxLDL
P<0.0001
P<0.0001
P<0.0001
5d
NRK52E
P=0.0037
P=0.0018
P=0.0011
5e
NRK49F
30
Gqi
Ang II+oxLDL+Gqi
P=0.0056
P<0.0001
P<0.0001
P<0.0001
P=0.0057
5f
NRK52E
MW (kDa)
P=0.0217
P=0.0350
P=0.0015
5g
NRK49F
Arb
Ang II+oxLDL+Arb
P=0.0090
P=0.0073
P=0.0477
5h
NRK52E
P=0.0150
P=0.0062
P=0.0042

Fig. 6

6a

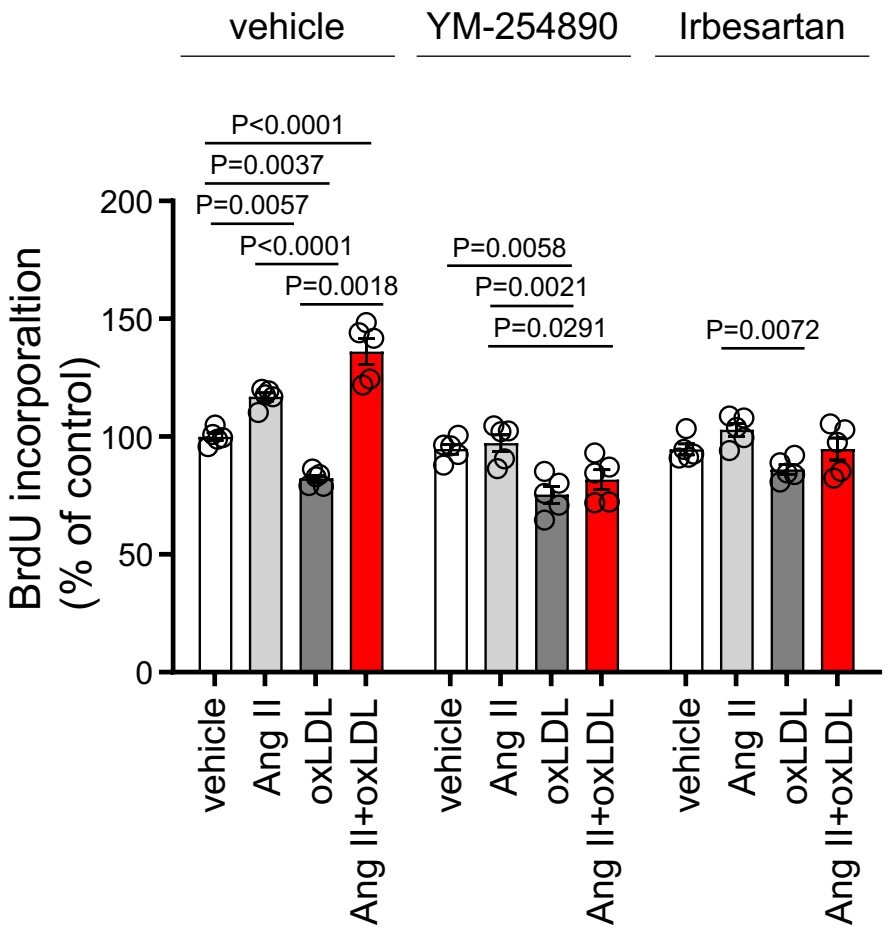
vehicle
YM-254890
Irbesartan
P<0.0001
P=0.0037
P=0.0057
P<0.0001
P=0.0018
P=0.0058
P=0.0021
P=0.0291
P=0.0072
BrdU incorporaltion
(% of control)
200
150
100
50
0
vehicle
Ang II
oxLDL
Ang II+oxLDL
vehicle
Ang II
oxLDL
Ang II+oxLDL
vehicle
Ang II
oxLDL
Ang II+oxLDL

6b

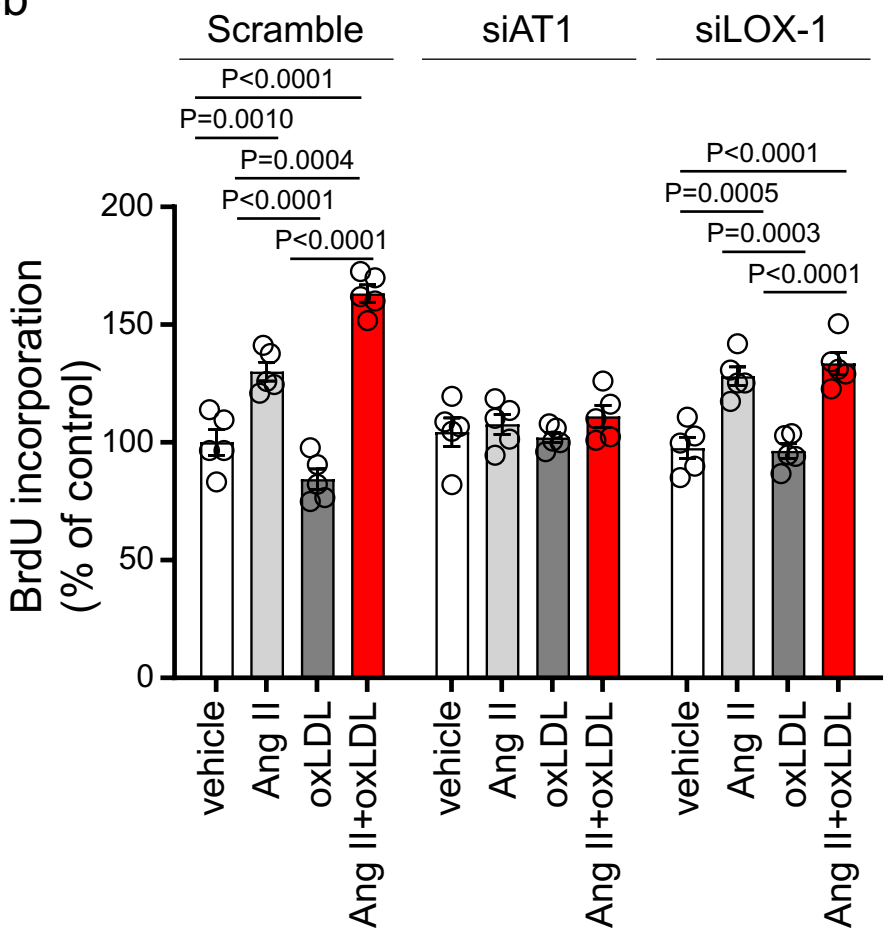
Scramble
siAT1
siLOX-1
P<0.0001
P=0.0010
P=0.0004
P<0.0001
P<0.0001
P<0.0001
P=0.0005
P=0.0003
P<0.0001
BrdU incorporation
(% of control)
200
150
100
50
0
vehicle
Ang II
oxLDL
Ang II+oxLDL
vehicle
Ang II
oxLDL
Ang II+oxLDL
vehicle
Ang II
oxLDL
Ang II+oxLDL

Fig. 7

7a

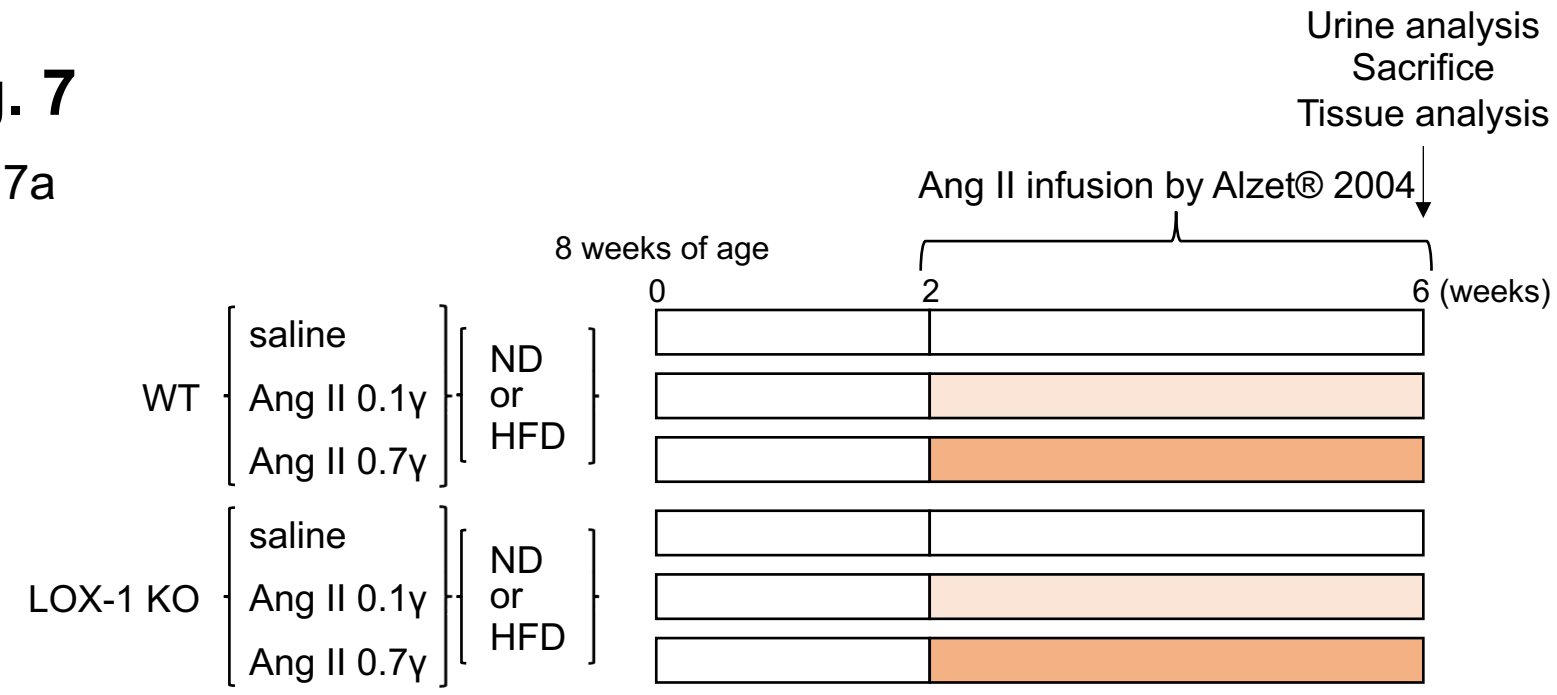

7b

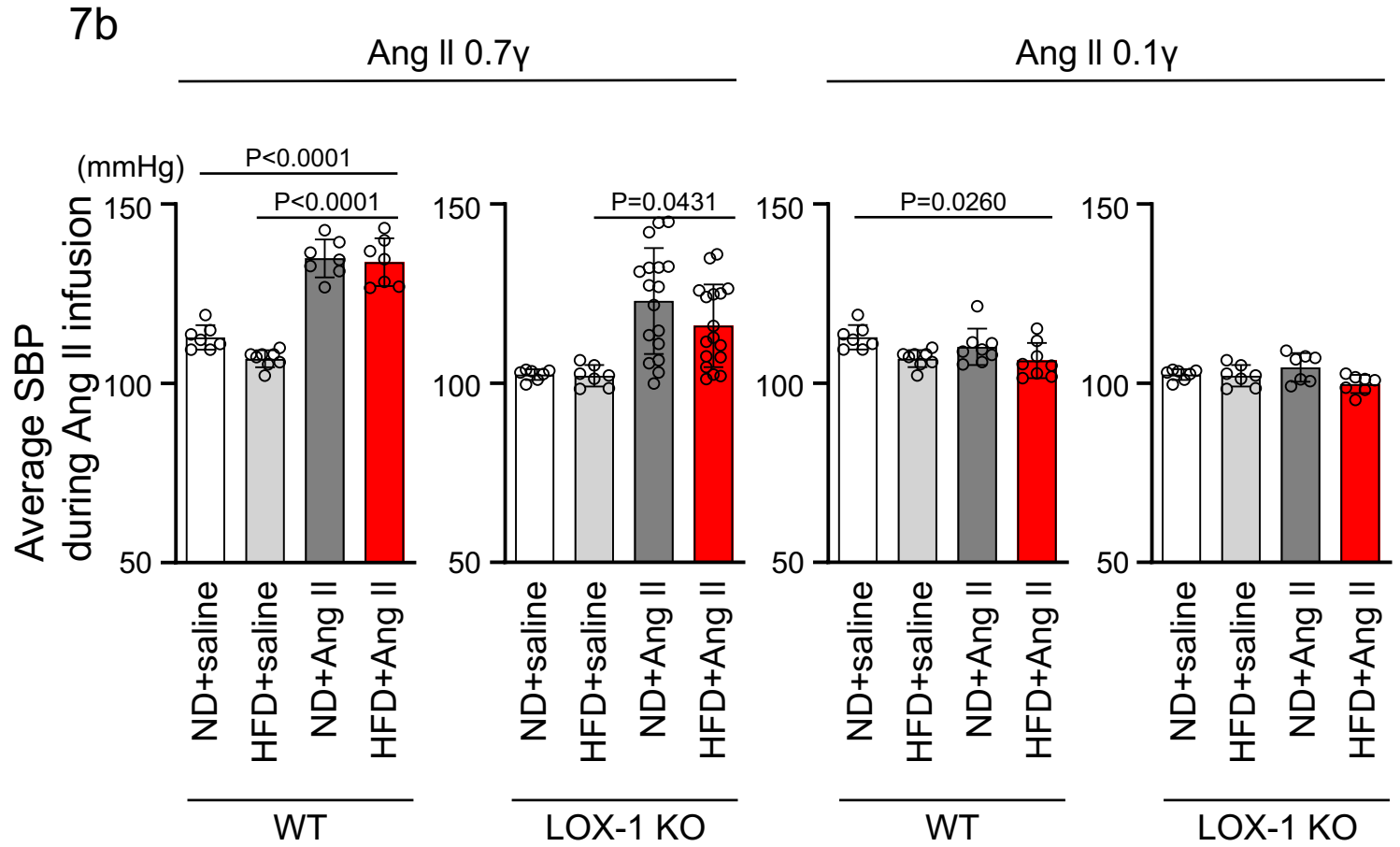

7c

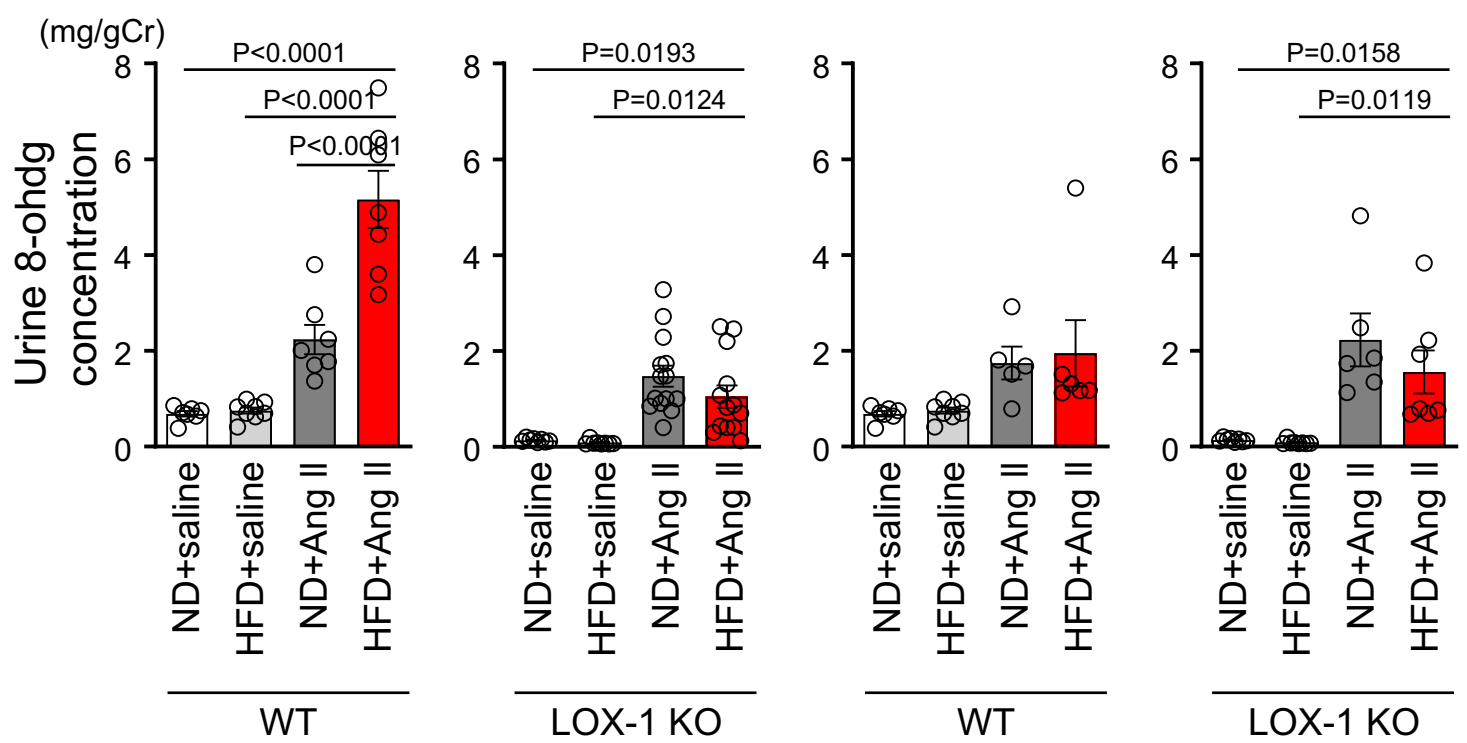

7d

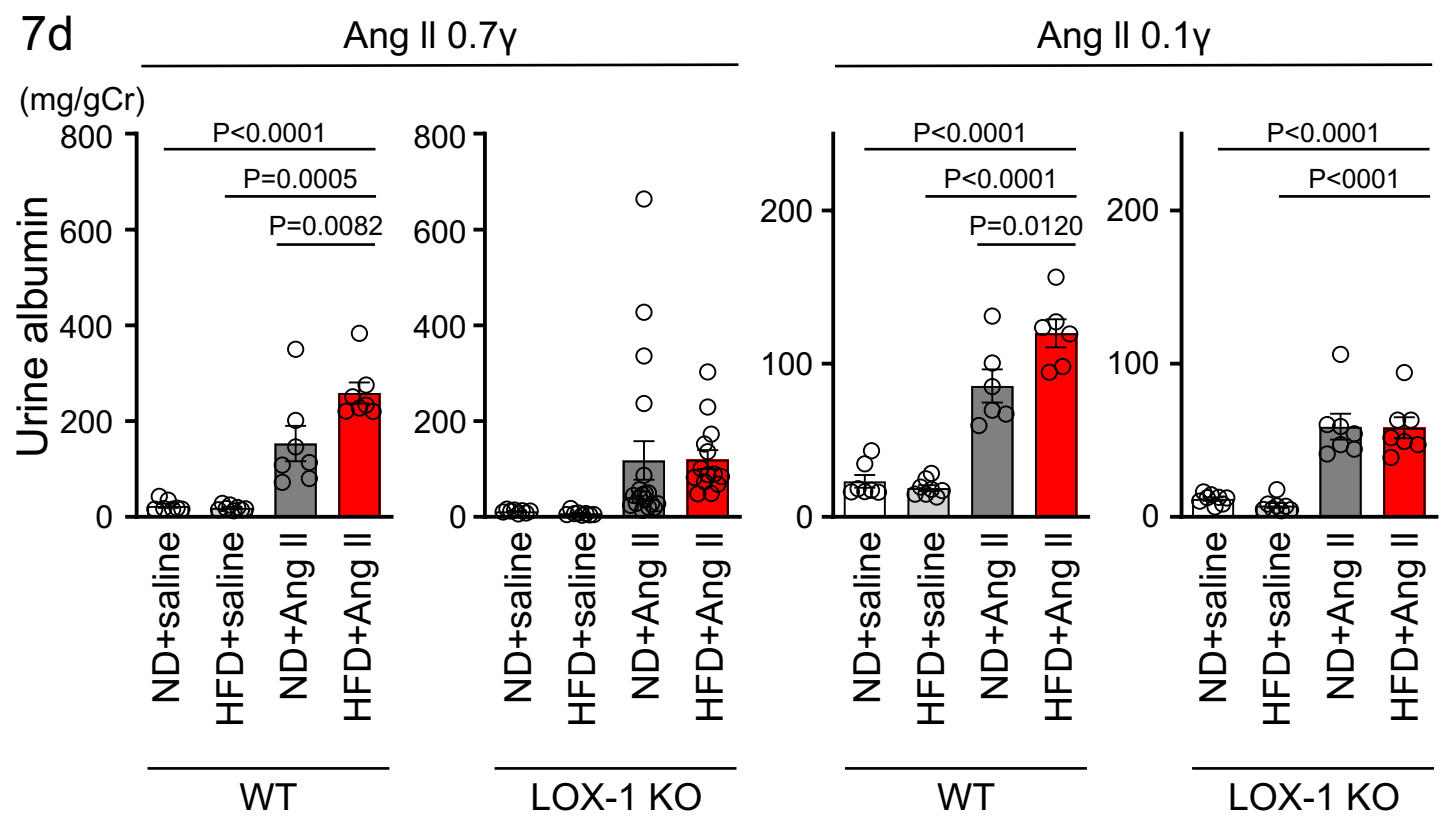

Fig. 8

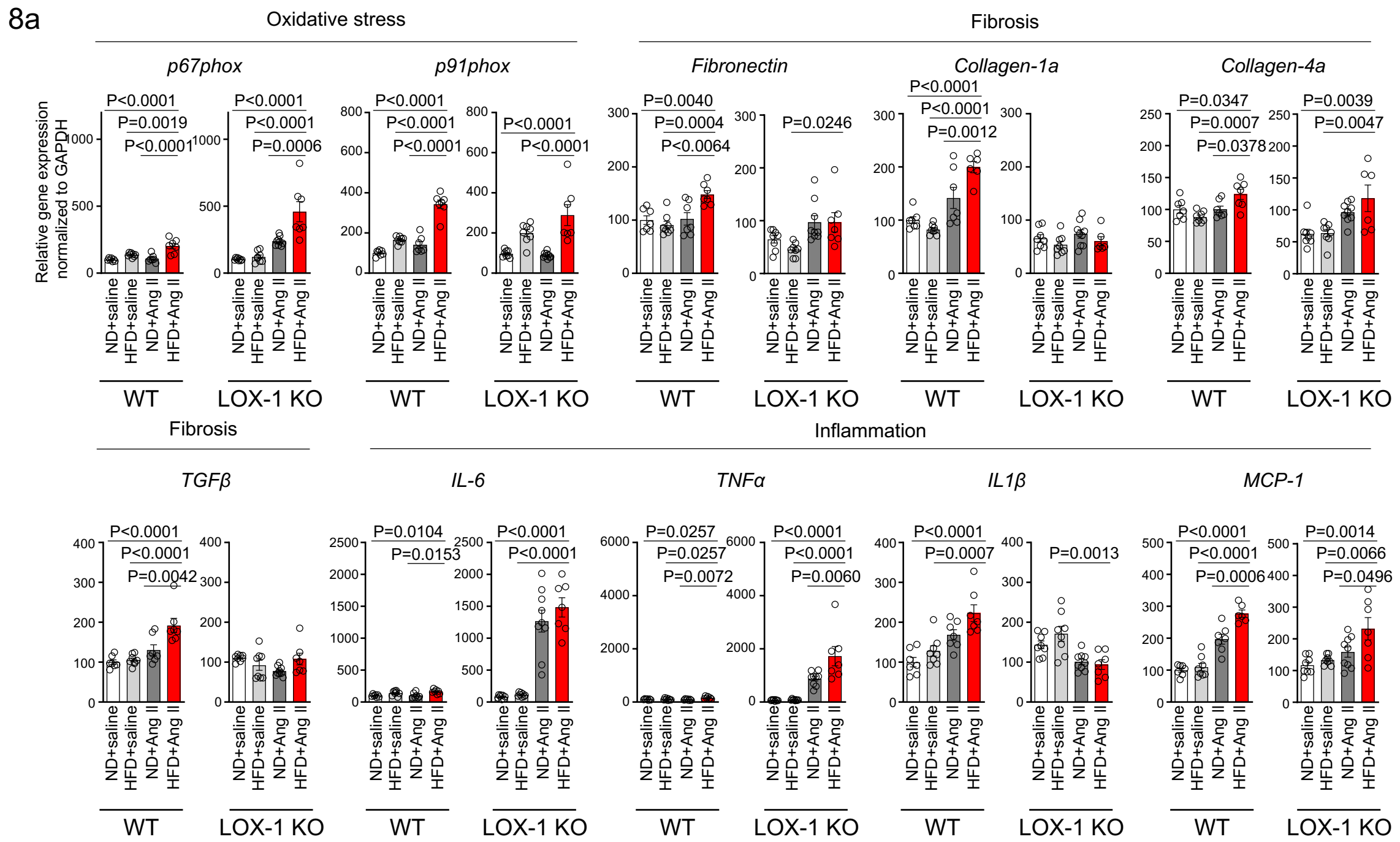
8a
Oxidative stress
Fibrosis
p67phox
p91phox
Fibronectin
Collagen-1a
Collagen-4a
Relative gene expression normalized to GAPDH
P<0.0001
P=0.0019
P<0.0001
P<0.0001
P=0.0006
P<0.0001
P<0.0001
P<0.0001
P<0.0001
P=0.0040
P=0.0004
P<0.0064
P=0.0246
P<0.0001
P<0.0001
P=0.0012
P=0.0347
P=0.0007
P=0.0378
P=0.0039
P=0.0047
ND+saline
HFD+saline
ND+Ang II
HFD+Ang II
WT
LOX-1 KO
Fibrosis
Inflammation
TGFβ
IL-6
TNFα
IL1β
MCP-1
P<0.0001
P<0.0001
P=0.0042
P=0.0104
P=0.0153
P<0.0001
P<0.0001
P=0.0257
P=0.0257
P=0.0072
P<0.0001
P<0.0001
P=0.0060
P<0.0001
P=0.0007
P=0.0013
P<0.0001
P<0.0001
P=0.0006
P=0.0014
P=0.0066
P=0.0496

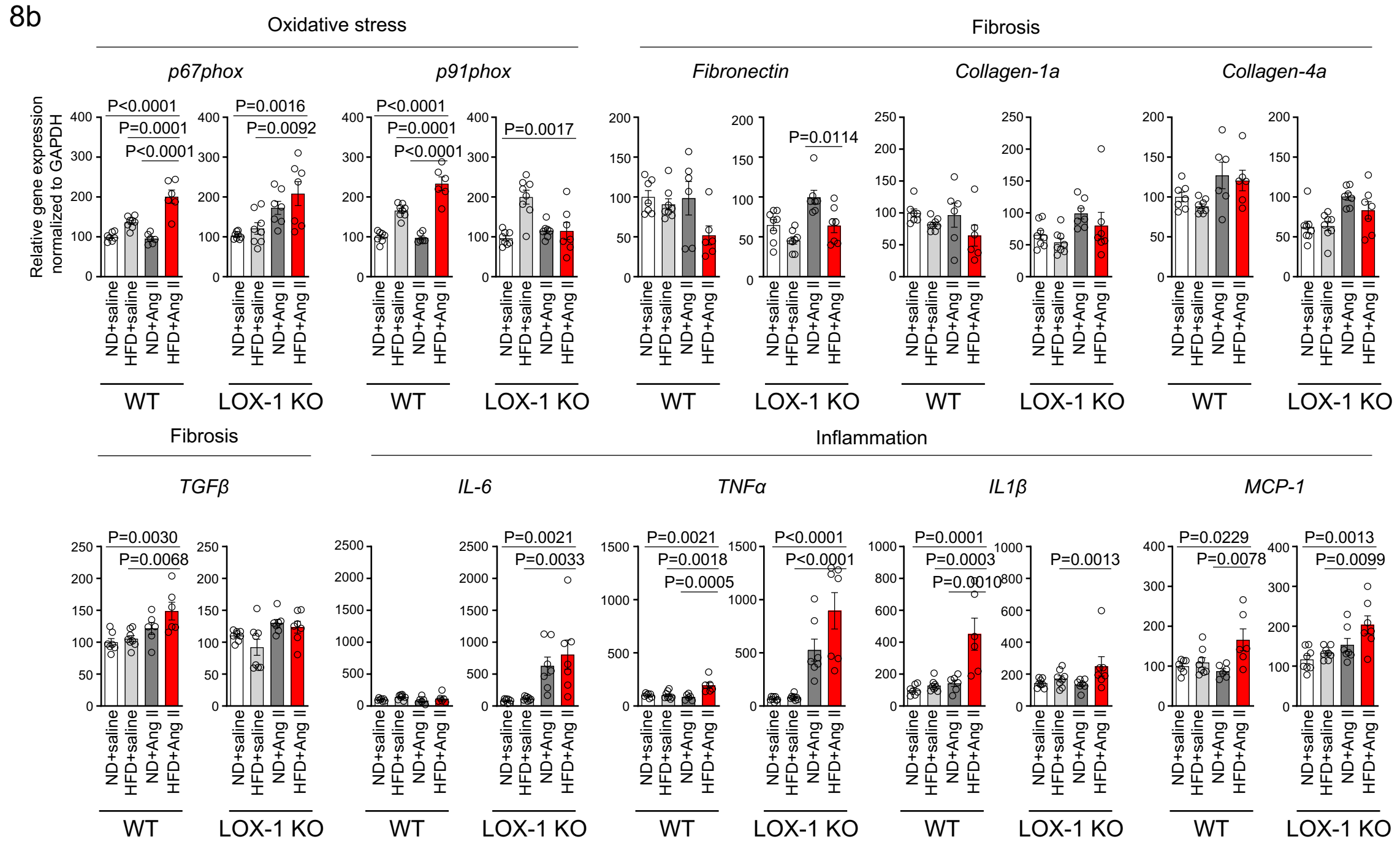
8b
Oxidative stress
Fibrosis
p67phox
p91phox
Fibronectin
Collagen-1a
Collagen-4a
Relative gene expression normalized to GAPDH
P<0.0001
P=0.0001
P<0.0001
P=0.0016
P=0.0092
P<0.0001
P=0.0001
P<0.0001
P=0.0017
P=0.0114
ND+saline
HFD+saline
ND+Ang II
HFD+Ang II
WT
LOX-1 KO
Fibrosis
Inflammation
TGFβ
IL-6
TNFα
IL1β
MCP-1
P=0.0030
P=0.0068
P=0.0021
P=0.0033
P=0.0021
P=0.0018
P=0.0005
P<0.0001
P<0.0001
P=0.0001
P=0.0003
P=0.0010
P=0.0013
P=0.0229
P=0.0078
P=0.0013
P=0.0099

Fig. 9

9a

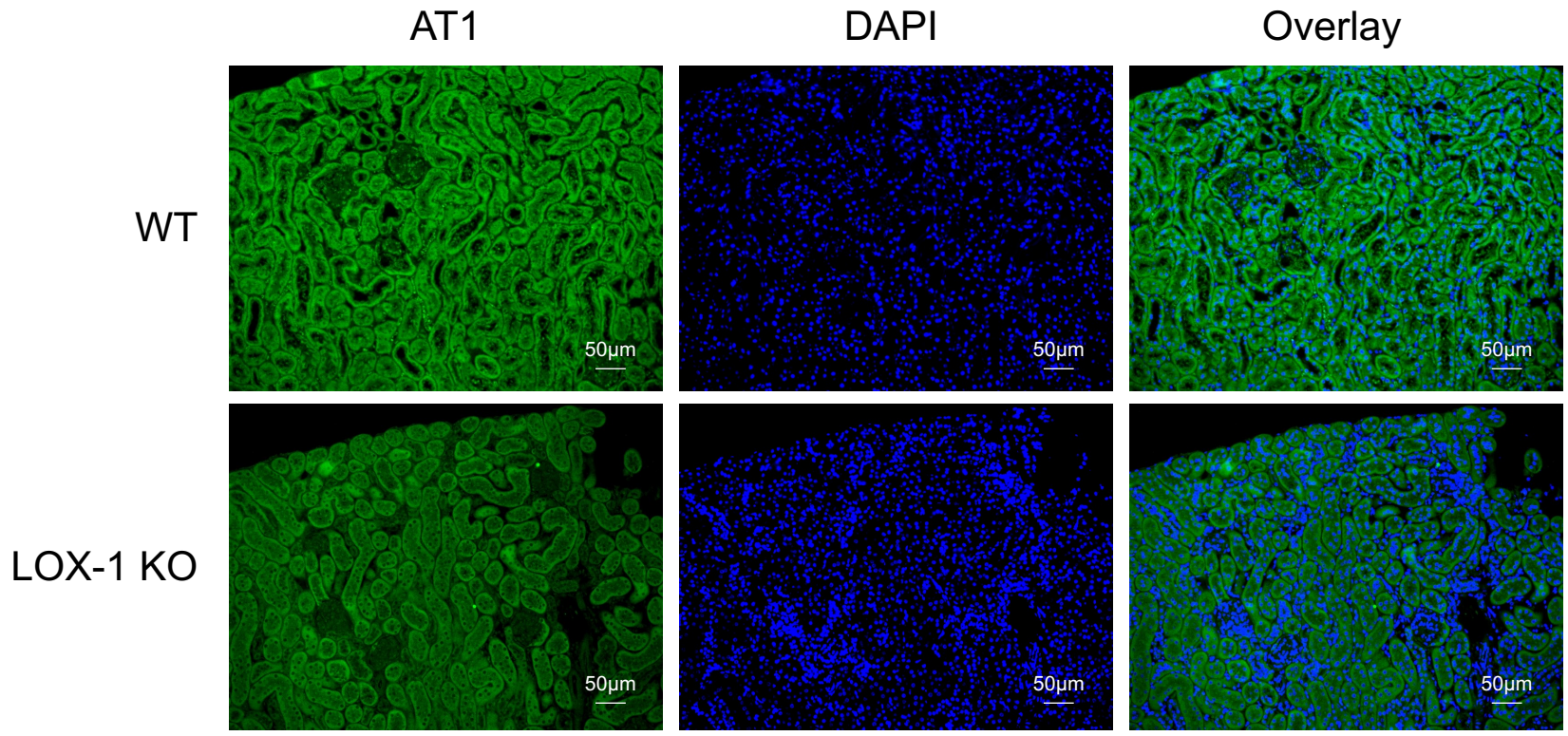
AT1
DAPI
Overlay
WT
LOX-1 KO
50μm

9b

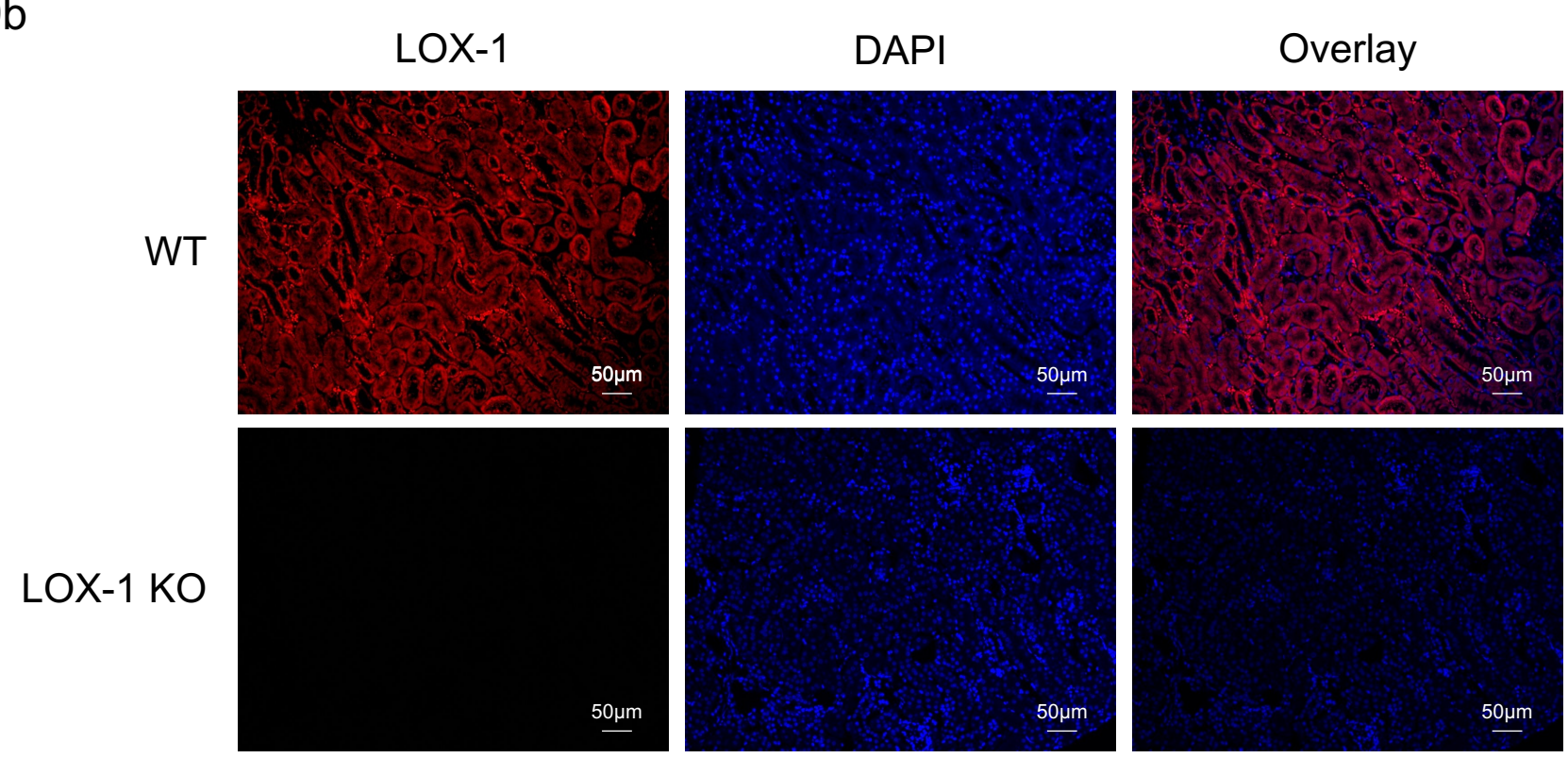
LOX-1
DAPI
Overlay
WT
LOX-1 KO
50μm

Fig. 10

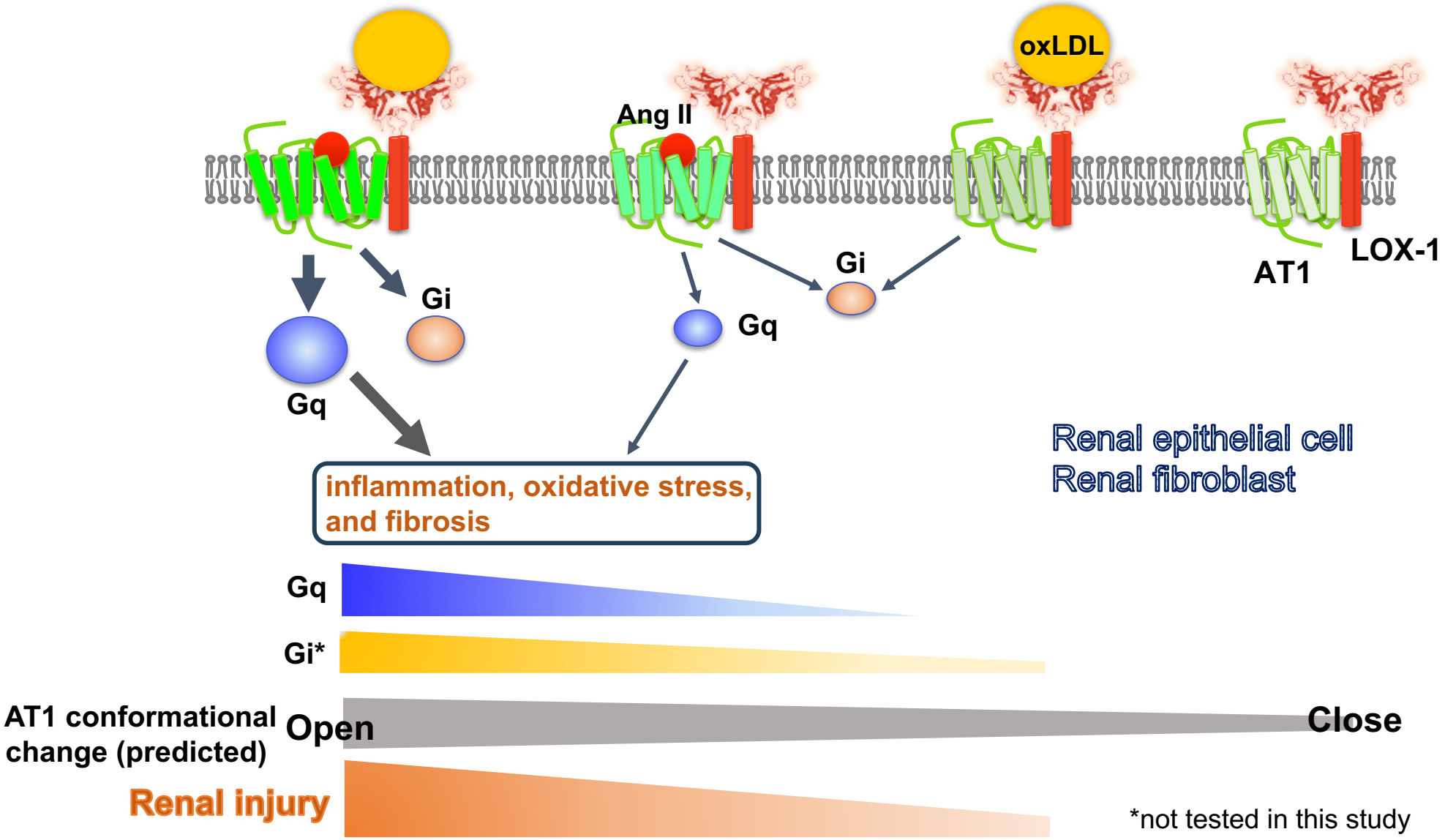
oxLDL
Ang II
Gi
Gq
Gi
Gq
AT1
LOX-1
inflammation, oxidative stress, and fibrosis
Renal epithelial cell
Renal fibroblast
Gq
Gi*
AT1 conformational change (predicted)
Open
Close
Renal injury
*not tested in this study

Fig. S1

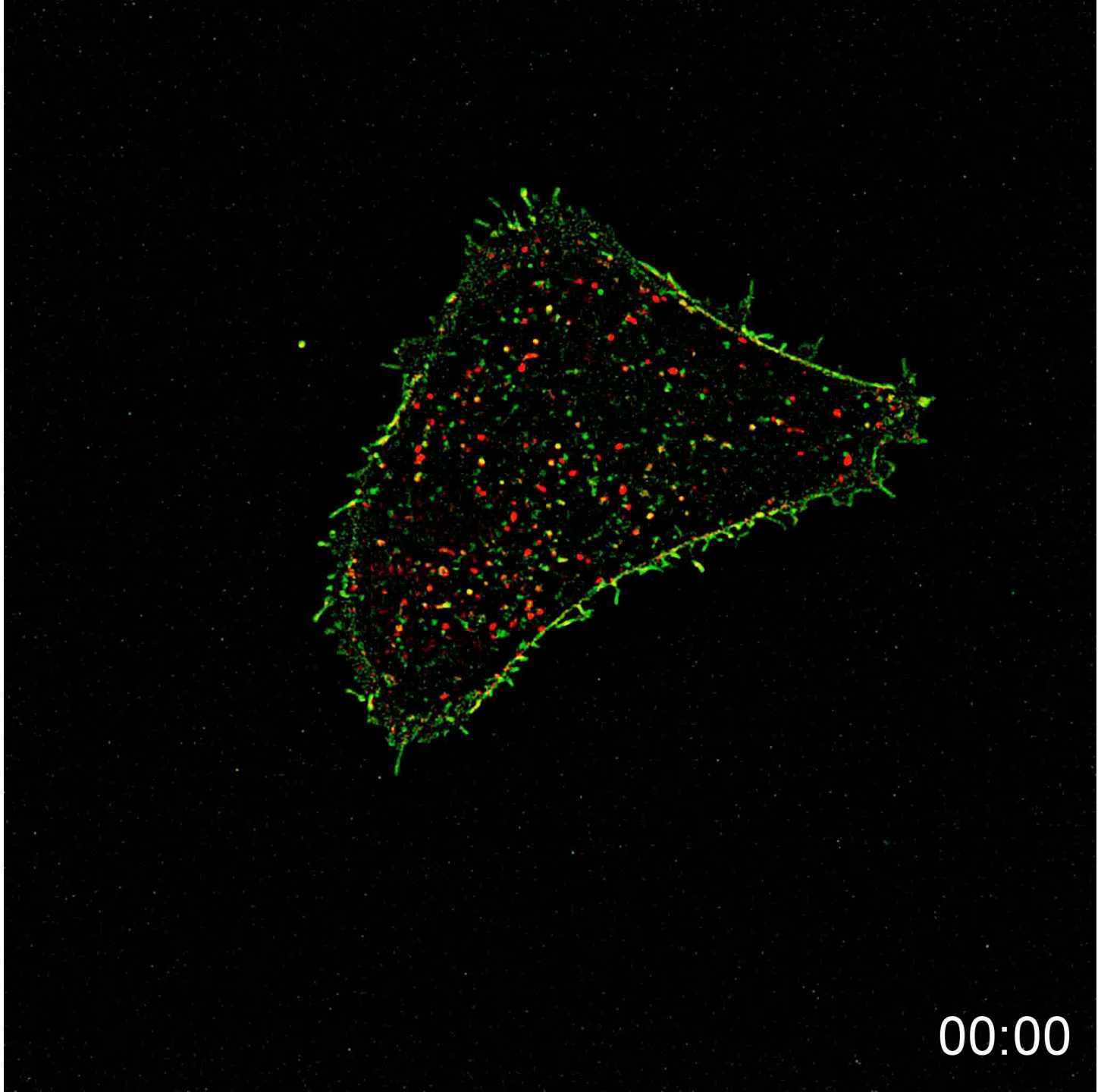
00:00

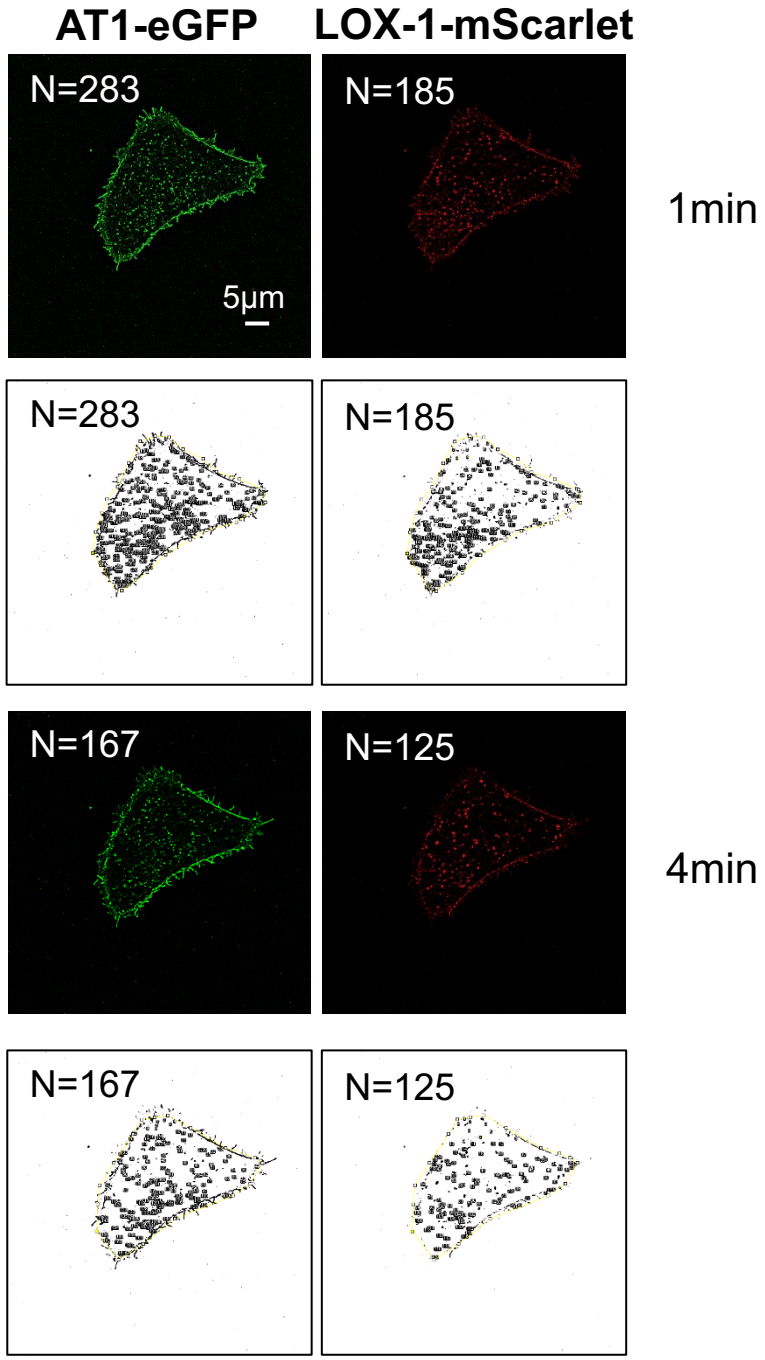
AT1-eGFP
LOX-1-mScarlet
N=283
N=185
5μm
1min
N=283
N=185
N=167
N=125
4min
N=167
N=125

Fig. S2

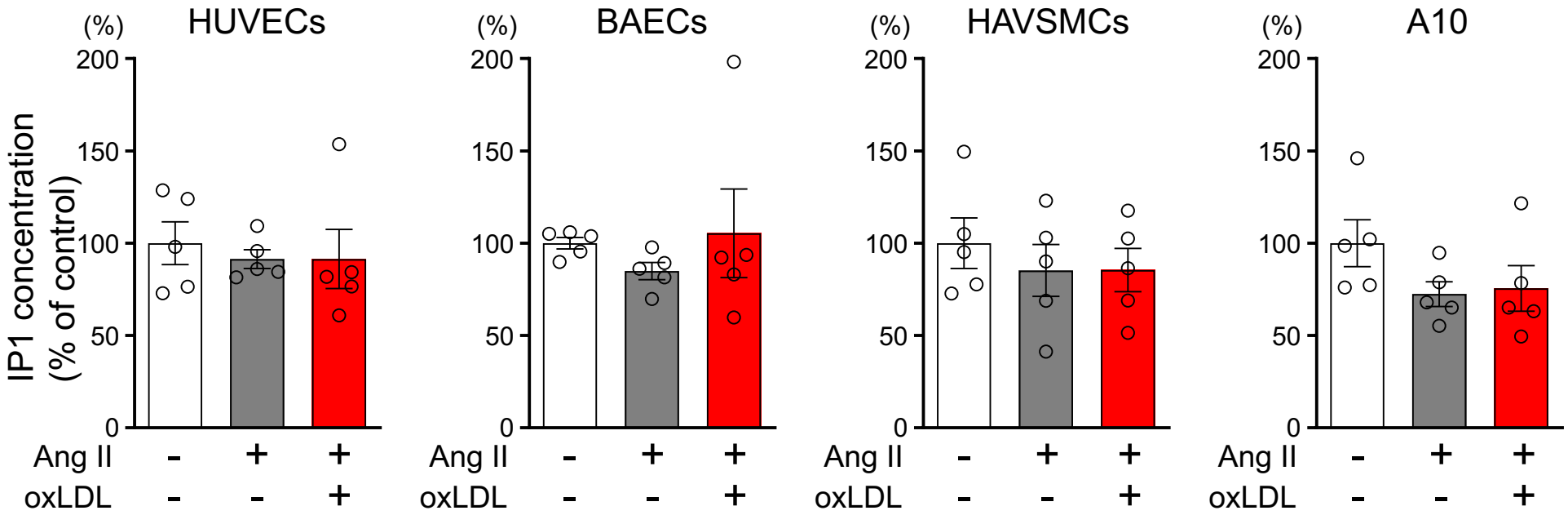
HUVECs
BAECs
HAVSMCs
A10
(%)
IP1 concentration
(% of control)
200
150
100
50
0
Ang II
oxLDL
-
+

Fig. S3

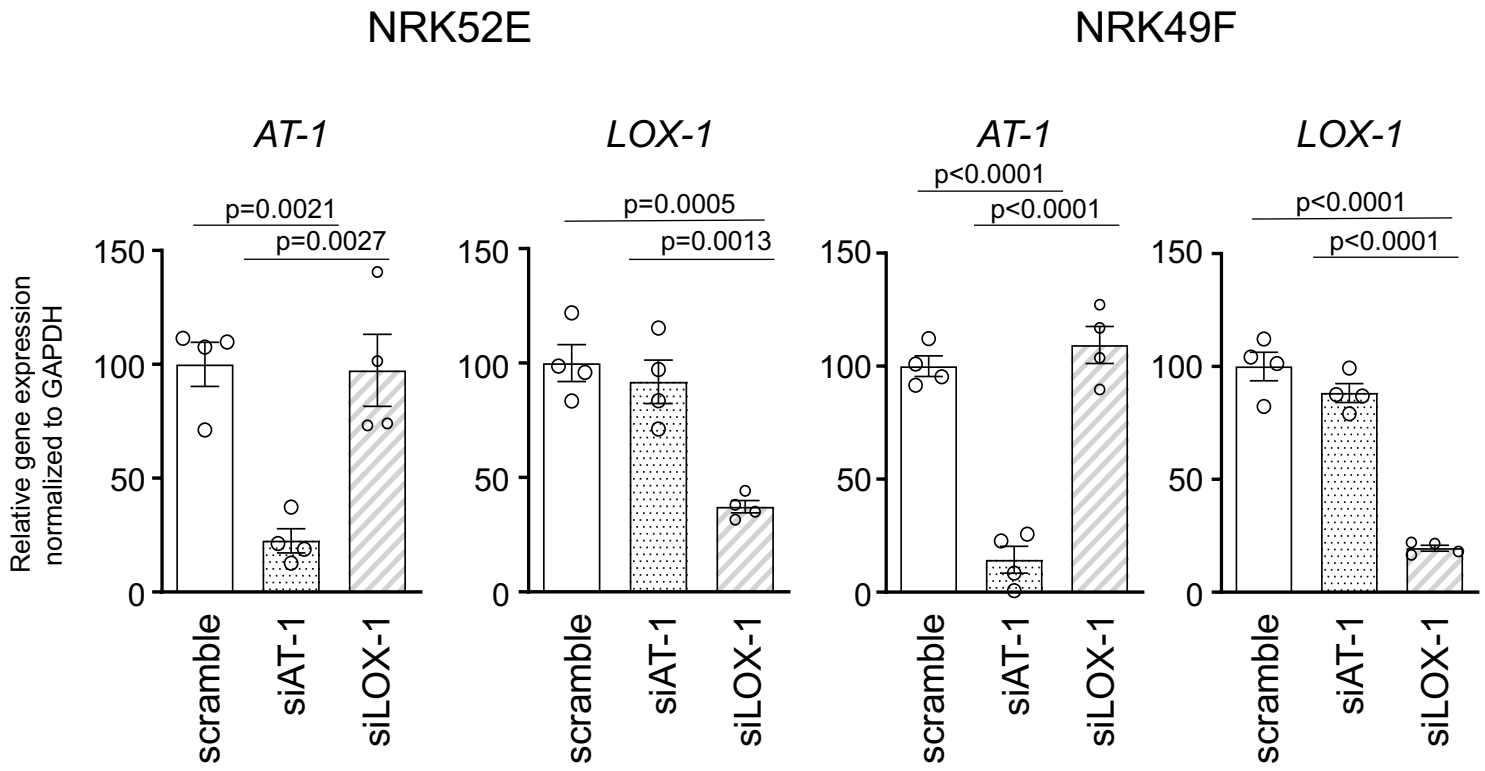
NRK52E
NRK49F
AT-1
LOX-1
AT-1
LOX-1
p=0.0021
p=0.0027
p=0.0005
p=0.0013
p<0.0001
p<0.0001
p<0.0001
p<0.0001
Relative gene expression normalized to GAPDH
150
100
50
0
scramble
siAT-1
siLOX-1

Fig. S4

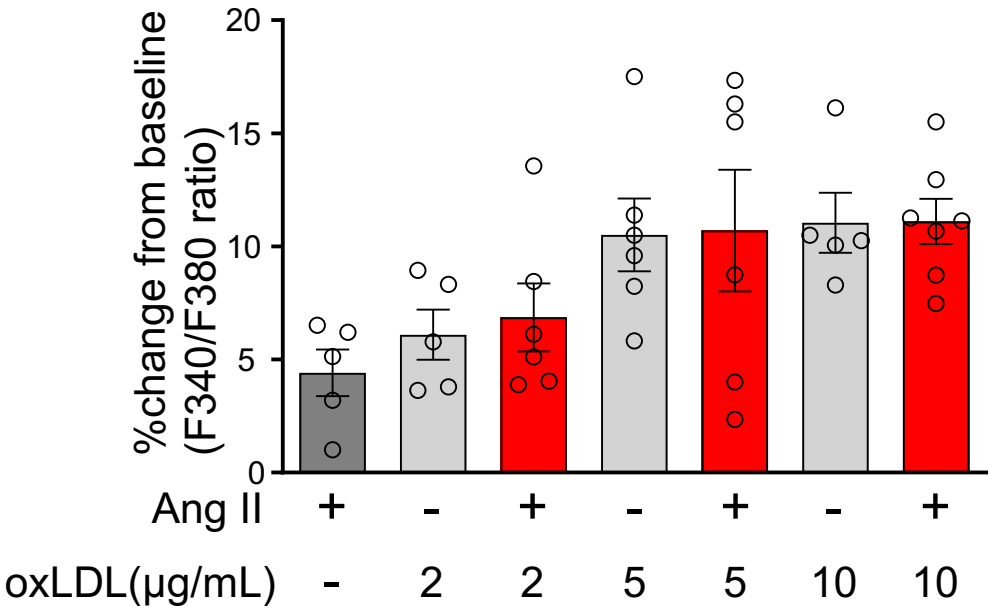
%change from baseline
(F340/F380 ratio)
20
15
10
5
0
Ang II
+
-
+
-
+
-
+
oxLDL(μg/mL)
-
2
2
5
5
10
10

Fig. S5

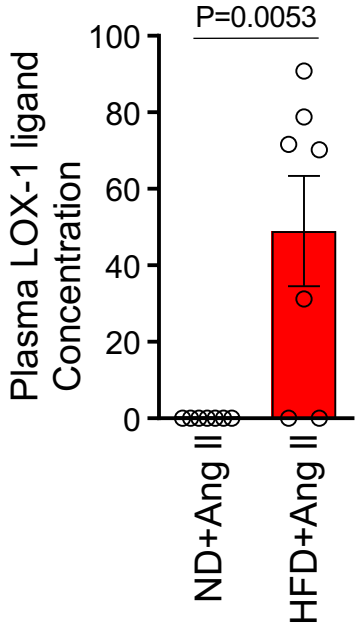
P=0.0053
Plasma LOX-1 ligand Concentration
100
80
60
40
20
0
ND+Ang II
HFD+Ang II

Fig. S6

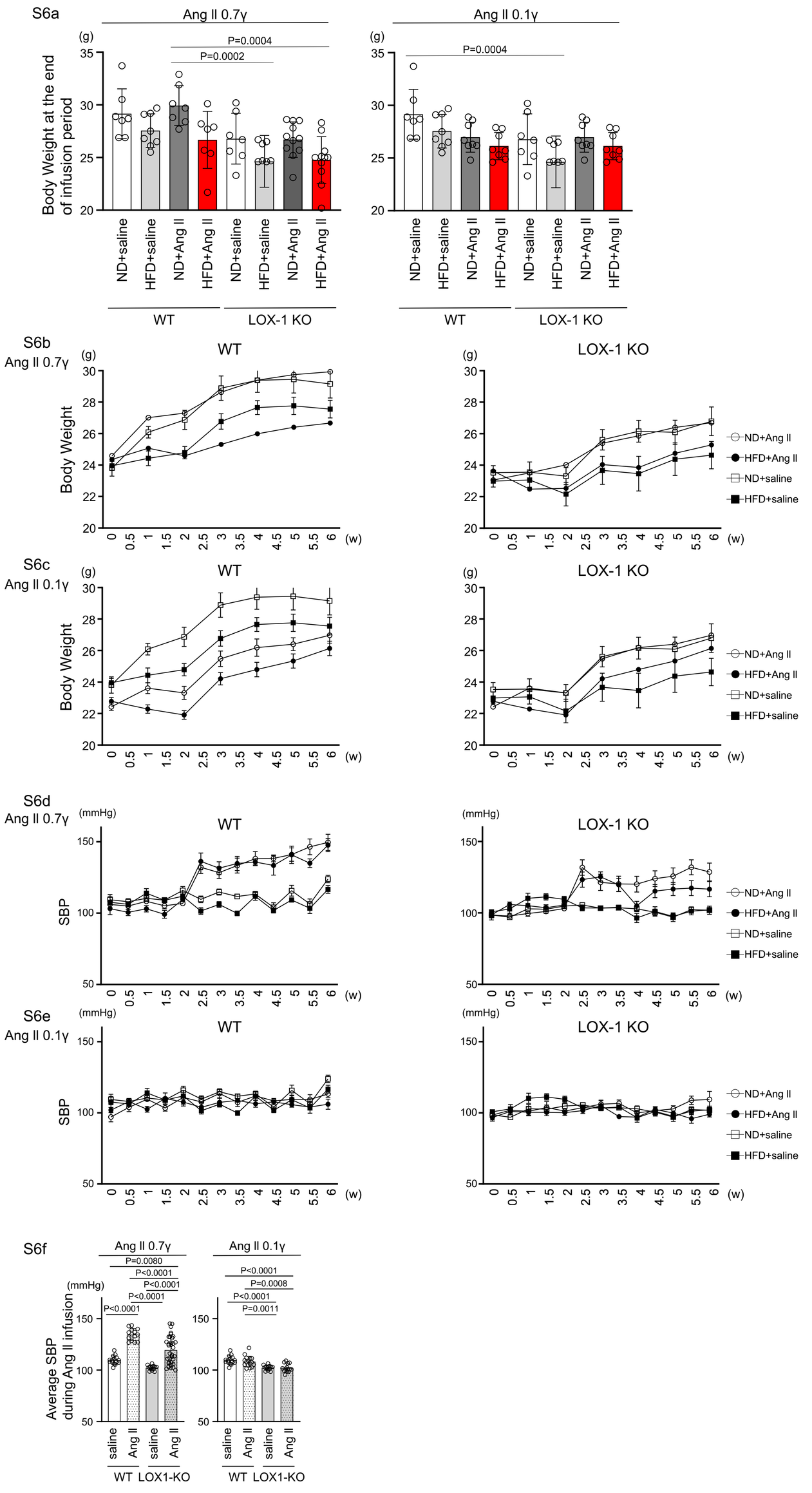
S6a
Ang II 0.7γ
Ang II 0.1γ
Body Weight at the end of infusion period
(g)
P=0.0004
P=0.0002
ND+saline
HFD+saline
ND+Ang II
HFD+Ang II
WT
LOX-1 KO
S6b
Ang II 0.7γ
S6c
Ang II 0.1γ
Body Weight
WT
LOX-1 KO
(w)
ND+Ang II
HFD+Ang II
ND+saline
HFD+saline
S6d
Ang II 0.7γ
S6e
Ang II 0.1γ
SBP
(mmHg)
S6f
Average SBP during Ang II infusion
P<0.0080
P<0.0001
P<0.0008
P=0.0011
saline
Ang II
WT
LOX1-KO

Fig. S7

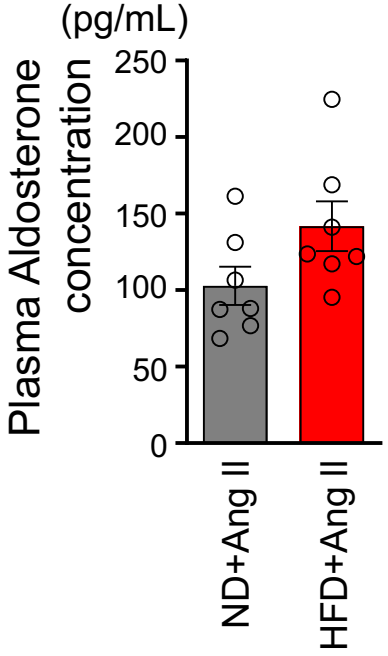
(pg/mL)
Plasma Aldosterone concentration
250
200
150
100
50
0
ND+Ang II
HFD+Ang II

Fig. S8

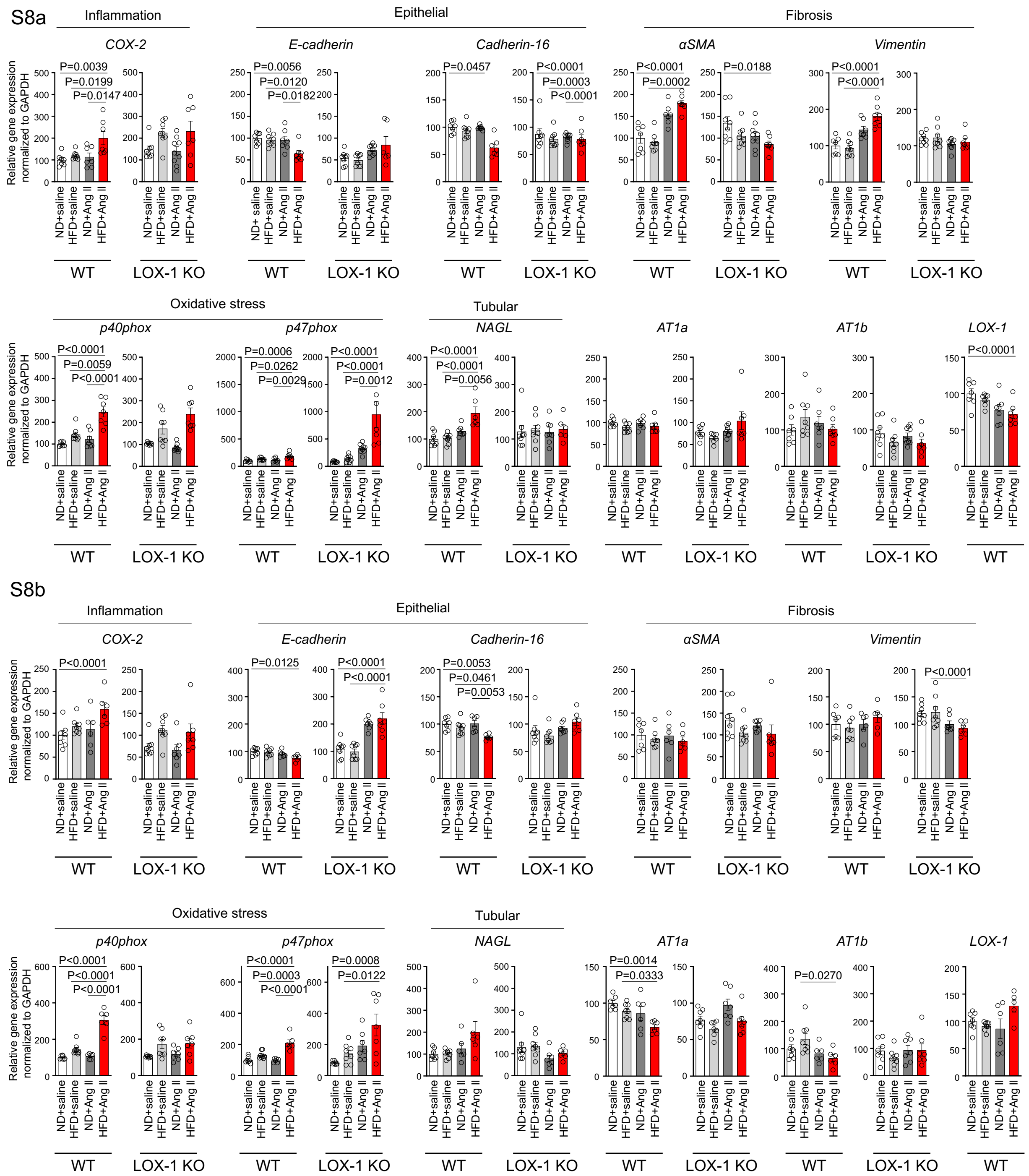
S8a
Inflammation
Epithelial
Fibrosis
COX-2
E-cadherin
Cadherin-16
αSMA
Vimentin
Relative gene expression normalized to GAPDH
P=0.0039
P=0.0199
P=0.0147
P=0.0056
P=0.0120
P=0.0182
P=0.0457
P<0.0001
P=0.0003
P<0.0001
P<0.0001
P=0.0002
P=0.0188
P<0.0001
P<0.0001
ND+saline
HFD+saline
ND+Ang II
HFD+Ang II
WT
LOX-1 KO
Oxidative stress
Tubular
p40phox
p47phox
NAGL
AT1a
AT1b
LOX-1
P<0.0001
P=0.0059
P<0.0001
P=0.0006
P=0.0262
P=0.0029
P<0.0001
P<0.0001
P=0.0012
P<0.0001
P<0.0001
P=0.0056
P<0.0001
S8b
Inflammation
Epithelial
Fibrosis
COX-2
E-cadherin
Cadherin-16
αSMA
Vimentin
Relative gene expression normalized to GAPDH
P<0.0001
P=0.0125
P<0.0001
P<0.0001
P=0.0053
P=0.0461
P=0.0053
P<0.0001
Oxidative stress
Tubular
p40phox
p47phox
NAGL
AT1a
AT1b
LOX-1
P<0.0001
P<0.0001
P<0.0001
P<0.0001
P=0.0003
P<0.0001
P=0.0008
P=0.0122
P=0.0014
P=0.0333
P=0.0270
WT
LOX-1 KO

Fig. S9

S9a

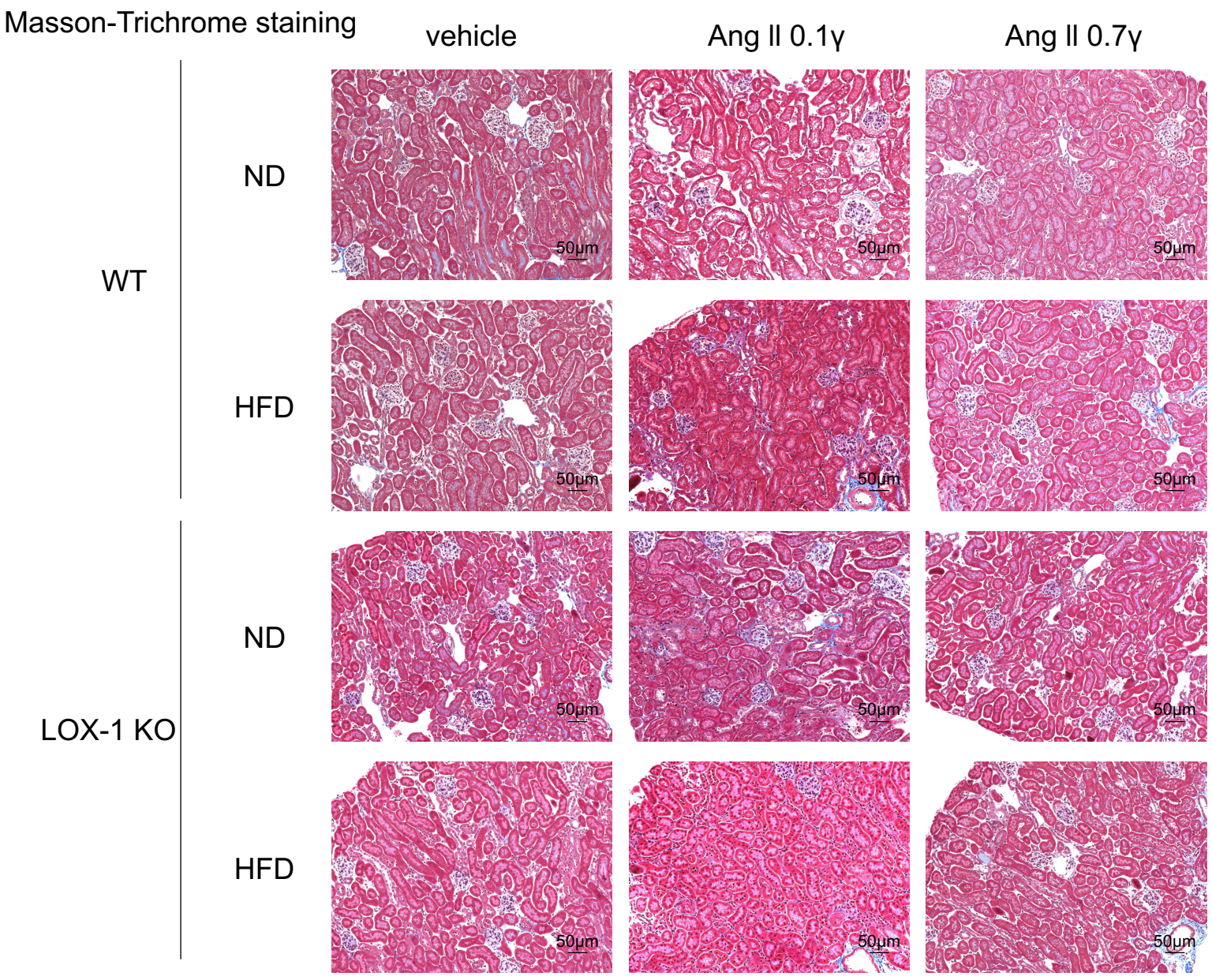

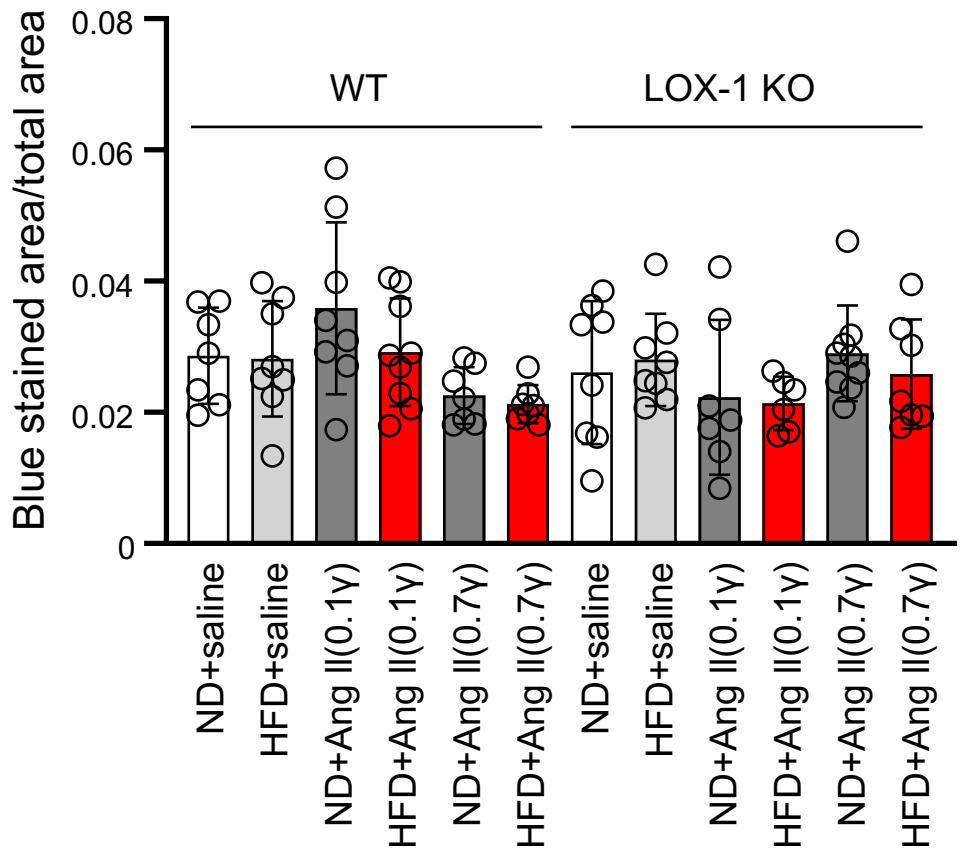
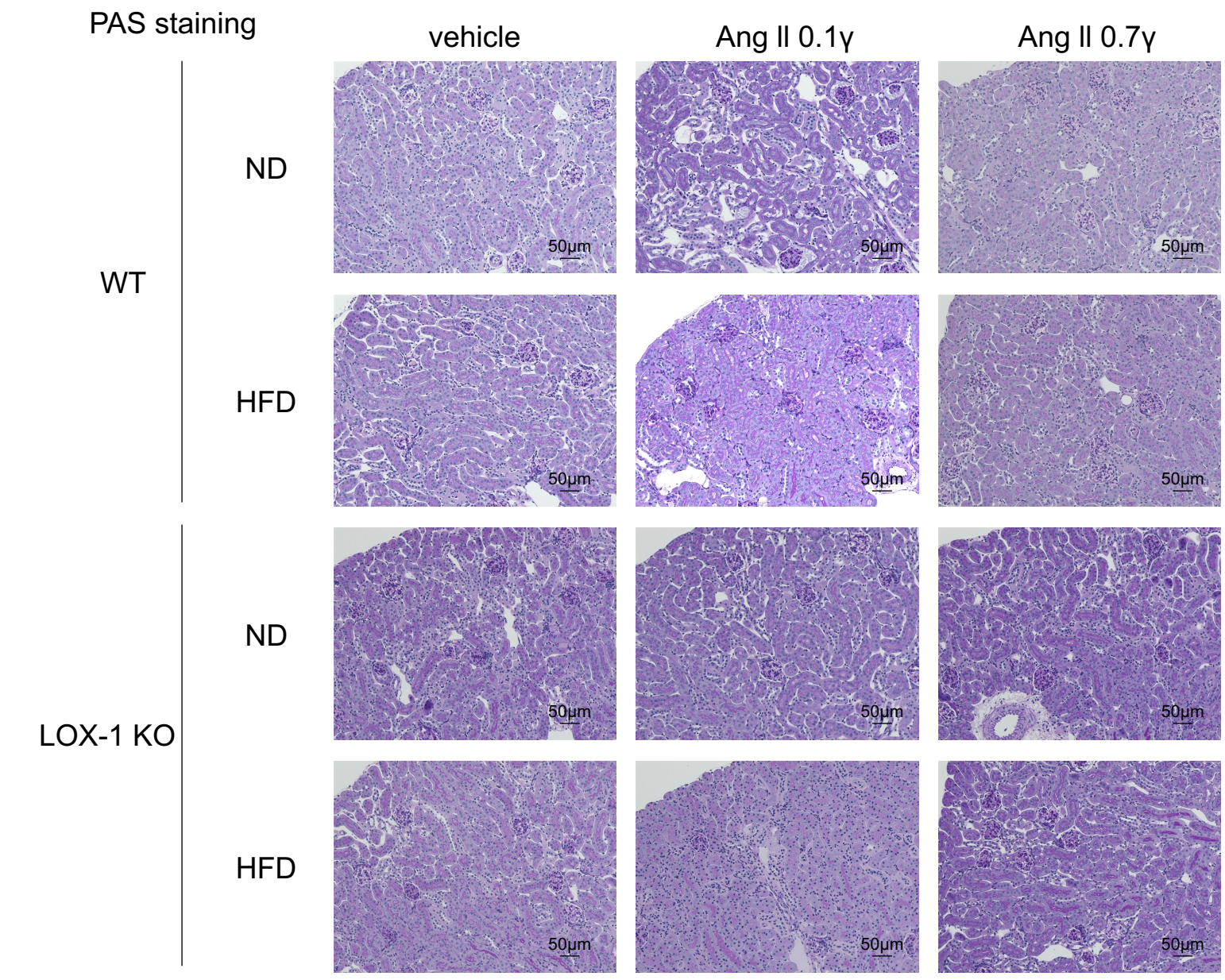
S9b